Distributed Properties of Asphaltene Nanoaggregates in Crude Oils: A Review

Murray R. Gray,* Harvey W. Yarranton, Martha L. Chacón-Patiño, Ryan P. Rodgers, Brice Bouyssiere, and Pierre Giusti

ACCESS | Metrics & More | Article Recommendations

ABSTRACT: The molecules in petroleum asphaltenes follow a molecular structure continuum similar to the rest of the oil but differ in the formation of nanoaggregates in solution. The nature of the aggregation, its size distribution, and dimensions of the nano-aggregates is still debated, and the impact of this aggregation on phase behavior, physical properties, and the processing of heavy petroleum fractions remains unclear. This review first discusses the role of nanoaggregates in the phase separation of asphaltenes, then examines the literature on subfractionation of the asphaltene fraction to define how different molecules partition. Efforts to measure the distribution of nanoaggregate size are summarized, and the roles of size distribution in the behavior of asphaltenes during sedimentation, emulsion formation, and refinery processing are examined. Finally, the

molecular basis for formation of a distribution of aggregate sizes/properties is considered. The molecular weight ranges as high as 40,000 Da but the size is below 100 nm. Although few direct experimental data are available for the distribution of aggregate properties, three behaviors indicate the importance of portions of the nanoaggregate population. The highest molecular weight aggregates are the least soluble, driving phase behavior when the asphaltenes are partially precipitated. A portion of these large aggregates are also most responsible for the stabilization of asphaltene films at oil–water interfaces, which stabilize oil-in-water emulsions. The vanadium and nickel species that are most resistant to removal during refining of vacuum residues are also found in the most aggregated fraction, although the stability of the aggregates at process temperatures is not yet proven. Average properties for the asphaltene fraction, including both free molecules and nanoaggregates, are sufficient for prediction of onset of asphaltene phase separation, gravity segregation, and properties such as density and viscosity.
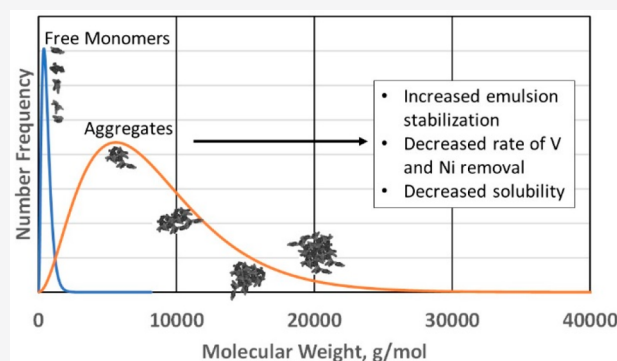
INTRODUCTION

Recent studies have provided unprecedented insight into the extreme diversity of molecular species in the asphaltene fraction of petroleum, which are based on extrographic separation followed by Fourier-transform ion-cyclotron resonance mass spectrometry (FT-ICR MS) combined with gas-phase fragmentation via infrared multiphoton dissociation (IRMPD).[1,2] This separation method first adsorbs the sample on silica gel at low concentration, then exhaustively extracts with a series of solvents. Analysis of these subfractions of asphaltenes overcomes, to some extent, the wide range of ionization efficiencies in atmospheric pressure photoionization, which gives a substantial bias toward the most aromatic components in unfractionated samples. The tens of thousands of species identified by FT-ICR MS indicate that the main range of the carbon number is from 10 up to 100 and double-bond equivalents from 1 to 40, although higher ranges have been reported depending on the sample and the instrument.[3,4] The distribution of molecular weight ranges from 250 to 1200 g/mol

in extrographic fractions from asphaltenes from different sources.

The maximum elemental ratios of components detected in subfractions of Athabasca bitumen asphaltenes (ATH) and Wyoming deposit asphaltenes (WY) are listed in Table 1, compared to the mean values determined by elemental analysis for the asphaltene samples, where available. The most hydrogen-rich molecules were in the O1 class, with H/C ratios well above the sample means. The most hydrogen deficient components were detected in the HC class, with a minimum H/C of 0.55 in ATH and 0.4 in WY. This range of H/C within the asphaltenes was much wider than previously observed in separation studies

Table 1. Sample Means (by Elemental analysis) and Maximum Elemental Ratios of Components Detected by FT-ICR MS of Extrographic Fractions Are Reported for Athabasca Bitumen Asphaltenes and Wyoming Deposit C_7-Asphaltenes[1,2,a]

Athabasca bitumen C_7-asphaltenes			
Element molar ratio	Sample mean ratio from elemental analysis[5,6]	Molecular maximum ratio	Class and fraction
Hydrogen, H/C	1.26	1.8	O_1 class in TOL
Oxygen, O/C	0.043	0.20	O_2S_1 in acetone subfraction
Nitrogen, N/C	0.016	0.13	N_1 in THF/MeOH
Sulfur, S/C	0.038	0.21	S_3 in TOL/THF
Vanadium, V/C	0.00032	0.031	Vanadyl etioporphyrin
Wyoming deposit C_7-asphaltenes			
Element molar ratio	Sample mean ratio from elemental analysis[7]	Molecular maximum ratio	Class and fraction
Hydrogen, H/C	1.06	1.3	O_1 class in TOL/THF
Oxygen, O/C	nr[b]	0.25	O_S in acetone subfraction
Nitrogen, N/C	0.005	0.091	N_1 in THF/MeOH
Sulfur, S/C	0.009	0.11	S_3 in HEP
Vanadium, V/C	nr[b]	0.031	Vanadyl etioporphyrin

[a]Class designations indicate hydrocarbon (HC) and number of oxygen, nitrogen, and sulfur atoms per molecule. O_1 indicates a single oxygen per molecule, as in furan, ketones, phenols, and ethers, and N_1 a single nitrogen per molecule as in pyrroles and pyridines. Thus, class O_1 groups are all the detected ions that contain carbon, hydrogen, and one oxygen atom. HEP is *n*-heptane. MeOH is methanol. THF is tetrahydrofuran. TOL is toluene. [b]nr: not reported.

(see Section 1). ATH and WY had average molar H/C ratios of 1.0 to 1.3, in the typical range observed in petroleum asphaltenes. Both ATH and WY were abundant in components containing sulfur, oxygen, and nitrogen, and in every case, the maximum ratios of S/C, O/C, and N/C in detected molecules were much higher than the experimental sample mean.

The range of identified molecular architectures is also exceptionally broad, including a diverse range of large polynuclear aromatic hydrocarbons (PAHs), polynuclear aromatic sulfur heterocycles (PASHs), and vanadyl porphyrins with structures also identified at the atomic level by noncontact atomic force microscopy (nc-AFM).[8,9] In unprocessed bitumen, a significant fraction of the asphaltene components could not be assigned a detailed chemical structure based on the nc-AFM images, although the molecular dimensions were determined.[8] Schuler et al.[10] reported nc-AFM structures with H/C ratios in the range from 0.41 to 0.60, far below the mean H/C = 1.04 (determined by elemental analysis) for the sample analyzed. Such disparity indicates a significant bias toward large unsubstituted aromatic compounds with low hydrogen content (low H/C ratio) due to factors such as their low extent of molecular aggregation, their quasi-planar molecular conformation, and the ability to assign their molecular structure.[11] The use of IRMPD on selected ions from FT-ICR MS showed that the fraction of large aromatic "islands" versus bridged or "archipelago" structures was highly dependent on sample source, the subfraction of asphaltenes, and the molecular weight of the selected precursor ions for fragmentation.[1,4,12] These studies of molecular architecture suggest a high level of structural diversity in the asphaltene components, although

the full range of molecular architectures is still not fully defined. Furthermore, asphaltene samples from diverse geological origin have revealed abundant compounds with *atypically* low aromaticity, for example, double bond equivalent (DBE) values below 12, but high heteroatom content. These species concentrate in interfacially active petroleum subfractions.[1,13−18] It is critical to highlight that vanadyl porphyrins, known to be island dominant, were used as naturally occurring internal standards in IRMPD. Their fragmentation behavior was consistent with the known island structures by NMR and AFM, confirming the validity of the IRMPD method for asphaltene structure interrogation.[12]

The complexity of the asphaltenes is compounded by their tendency to self-associate. The presence of molecular aggregates in asphaltenes from crude oil and in solutions of asphaltenes in solvents like toluene has been proposed for many years.[19,20] Separations that support the presence of stable molecular aggregates, indicating colloidal behavior, include ultracentrifugation,[21] nanofiltration,[22] and membrane dialysis.[23] Each of these physical separations gives a fraction enriched in nano-aggregates and a highly depleted fraction. Direct detection of nanoaggregates has been reported by mass spectrometry[24] and AFM.[25] A variety of indirect methods have been used to infer the presence of nanoaggregates, usually as a function of concentration. Yarranton et al.[26] compared a range of methods for characterizing nanoaggregates of asphaltenes in solution. They reported an average molecular weight on the order of 10,000 to 20,000 g/mol, compared to a monomer mass ranging from 250 to 1200 g/mol. They found that small-angle X-ray scattering and dynamic light scattering gave molecular weights for aggregates that were 10 times larger. The physical dimensions of the nanoaggregates by different methods were in the range of 5 to 20 nm, with the upper bound determined from nanofiltration and the lower bound from membrane diffusion.

The extreme diversity of asphaltene components shows that the concept of an average molecule with average behavior can be extremely misleading. Nanoaggregates may also show wide diversity if they are formed by selective interactions of their component molecules. Alternatively, if molecules aggregate due to nonselective interactions, then aggregates will give significant averaging of the component molecular properties. In either case, any solution of asphaltenes in their native crude oils or in solvents will include both individual molecules and nano-aggregates of dimers, trimers, tetramers, and so on, with a distribution that depends on the chemistry of the components.

This review was prompted by a practical question: When do the details of asphaltene aggregation matter, beyond the obvious challenge that aggregation poses to molecular-level characterization? The objective is to probe the behaviors of asphaltenes, which have been linked to the presence of nanoaggregates, to define when the distributions of nanoaggregate behavior are important and where possible to understand the molecular contributions to these behaviors. We begin with the macroscopic separation of asphaltene-rich phases during production and refinery processing to define the nature of the asphaltenes. The potential contribution of nanoaggregation to the phase separation is examined to determine whether a distribution of nanoaggregate properties could be significant. The results of fractionation of asphaltenes using solvent mixtures such as *n*-heptane + toluene are then examined from the same perspective. Next, the results of experiments on the direct measurement of nanoaggregate composition and properties are reviewed to seek evidence of a distribution of properties or behavior. Interactions
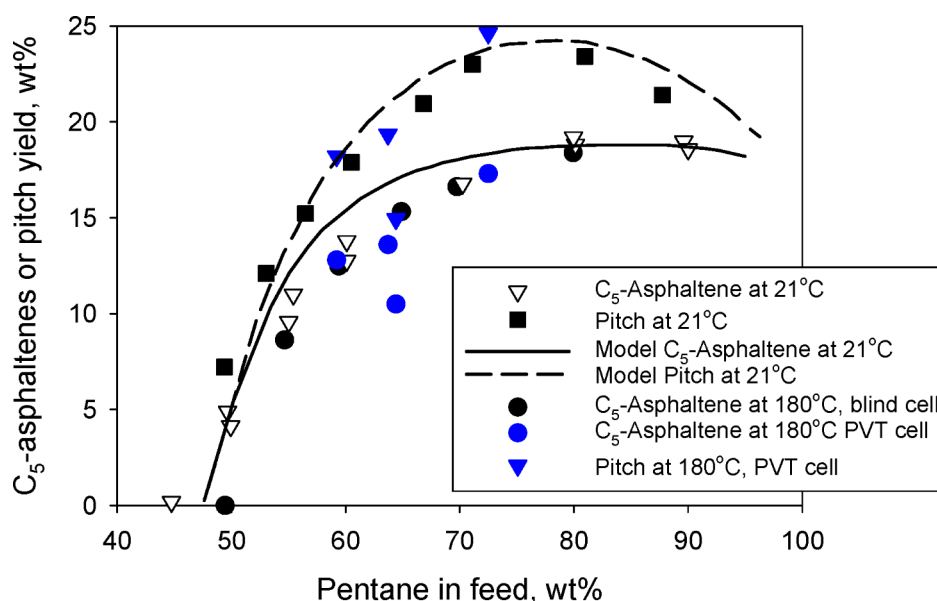
Figure 1. Yield of C_5-asphaltene-rich heavy phase (pitch) and C_5-asphaltenes from Athabasca bitumen-n-pentane mixtures at 21 °C and 0.1 MPa and at 180 °C and 4.8 MPa. The yields of pitch are reported on a n-pentane-free basis. Model curves are from a modified regular-solution theory fit to the data at 21 °C and 0.1 MPa.[33,34]

of asphaltenes with oil−water interfaces and solid surfaces are examined for evidence of an important role for a distribution of nanoaggregate surface properties. The effect of refinery process reactions on the asphaltene components and the resulting changes in nanoaggregation are examined to provide insight into the controlling molecular interactions. Finally, the range of potential nanoaggregate structure is considered based on the expected intermolecular forces between specific classes of asphaltene components and is tested against the available data from actual asphaltenes.

The exclusive focus of the review is on petroleum materials, including crude oil, bitumen, and their derived fractions such as vacuum residue and asphalt cement. The solubility definition of asphaltene, as a fraction soluble in toluene and insoluble in n-pentane or n-heptane, originated with coal-derived liquids and has also been applied to pyrolysis tars from steam cracking of naphtha and from lignocellulosic biomass. These materials have dramatically different origins and compositional distributions from petroleum samples and are not be considered here.

1. INSIGHTS FROM ASPHALTENE PHASE SEPARATION AND MATERIAL PROPERTIES

1.1. The Nature of Phase Separation. The precipitation or phase separation of the asphaltenes is one of the most important features of this material in production and processing of petroleum. To put the role of nanoaggregates into context, we need to define how this aggregation at the molecular scale is related to the macroscopic observations of phase separation, if at all. We begin with the nature of the macroscopic separation.

Many experiments on phase separation of asphaltenes are conducted at ambient temperature, where the asphaltene phase appears as solid particles dispersed in a continuous liquid phase. This process is often described as precipitation or flocculation because the second phase that forms is a powdered solid, and the radius and morphology of the solid particles can be modeled through flocculation kinetics.[27−29] Once asphaltene separation begins, the formation of particles of dimensions from 200 nm to 2 μm is almost instantaneous. These primary particles then

flocculate to give porous particles with mean diameters up to 400 μm depending on the concentration and shear forces.[29−31] Detailed studies of asphaltene precipitation show that the kinetics of the primary particle formation are extremely fast, with a rapid increase in dimension from aggregated molecules ca. 5− 20 nm to primary particles of diameters up to 400 μm in a fraction of one second.[29] This behavior can only be explained as a phase transition, not as an extended molecular aggregation process wherein dissolved molecules associate stepwise with the existing aggregates. This conclusion contradicts a common trope in the literature on asphaltenes, which conflates nano-aggregation with macroscopic phase separation.

Consistent with a phase transition, the asphaltenes separate not only as solids but as part of a liquid phase at higher temperatures. For example, as the temperature is increased above room temperature, the addition of n-alkane to a crude oil yields separation of a heavy liquid phase that is enriched in asphaltene components, or pitch, rather than a flocculated solid material.[32−34] The transition temperature for Athabasca bitumen is approximately 90 °C; below this temperature, the heavy asphaltene-rich phase consists of porous flocculated solid in a continuous liquid phase, while above this temperature it is a separate liquid phase with a distinct interface.[33,34] The data of Figure 1 show that both solid- and liquid-phase separations give equivalent yields of n-pentane insoluble asphaltenes (C_5-asphaltenes) in the heavy phase. At both 21 and 180 °C, the pitch phase contains significant amounts of maltenes and pentane solvent, which is consistent with a phase separation process. For example, a mixture of 36 wt % bitumen and 64 wt % n-pentane at 180 °C and 4.8 MPa gave a heavy pitch phase containing 52 wt % C5-asphaltenes, 22 wt % maltenes, and 26 wt % n-pentane. In contrast, the n-pentane content of the pitch at 21 °C was much lower, in the range of 3 wt %.[35]

Although the definition of asphaltenes as a class of molecules that are soluble in toluene and insoluble in n-pentane or n-heptane gives the impression that this fraction of petroleum has a coherent chemical definition, its definition by a liquid−liquid phase separation is highly nonselective. Like any multi-

Table 2. Apparent Asphaltene Molecular Weights Used in Selected Phase Behavior Models Applied to Asphaltene Precipitation

| Model	Number of asphaltene fractions	Average MW (g/mol)	MW range (g/mol)	Comment
MRS[34]	30	3000	800−15000	Matching onsets; yields same MW values for all oils
CEOS[33]	5	2000	1200−2800	Matching onsets; yields same MW values for all oils
PC-SAFT[42]	3	1300−2700	1100−3800	Matching onsets; yields MW values depended on oil and assumed aromaticity
PC-SAFT[43]	1	700−4000	−	Matching onsets only; MW values depend on oil
CPA[44]	1	1800	−	Matching onsets; yields same MW values for all oils
CPA[45]	2−3	−	2900−5600	Matching onsets; yields MW range depends on oil
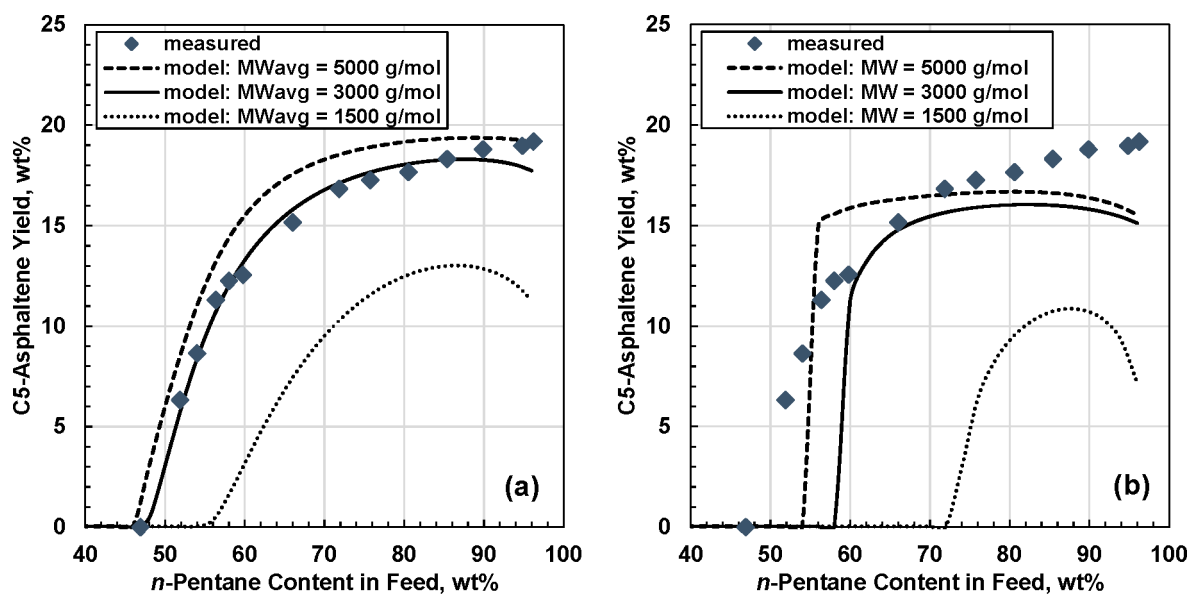
Figure 2. Effect of asphaltene molecular weight distribution on the predicted onset and yield of asphaltene precipitation from an *n*-pentane diluted bitumen at 21 °C and 0.1 MPa: (a) effect of average molecular weight in a molecular distribution and (b) effect of molecular weight with no distribution. Measured data from Johnston et al.[33]

component separation, some components appear almost exclusively in the *n*-alkane-rich phase, while others appear mainly in the asphaltene-rich phase and others in both phases.[36] The continuum of components in petroleum always gives rise to significant overlap between separated fractions. Asphaltene flocculation and subsequent precipitation occludes alkane-soluble compounds inside nanoaggregate networks that are difficult to remove even through extended washing with alkane solvents. Those compounds typically reveal lower carbon numbers, double bond equivalents, and levels of heteroatoms (i.e., N and O) compared to the bulk of the alkane-insoluble asphaltenes.

The asphaltene-rich phase is a solution of both aggregated and molecular species, whereas the *n*-heptane-soluble maltene fraction gives little evidence for aggregation based on vapor-pressure osmometry, gel permeation chromatography, and fluorescence spectroscopy.[37−40] When the asphaltene fraction is prepared in the laboratory, the flocculated solids are washed with *n*-heptane or *n*-pentane, then dried to remove residual solvents. The impact of the wash step is method dependent. A brief wash will remove entrained liquid between the asphaltene particles, while more exhaustive Soxhlet extraction will remove the most alkane-soluble components from the asphaltene phase. Industrial separation of asphaltene-rich phases is remarkably similar. Countercurrent washing is used to clean asphaltenes that are precipitated at low temperatures and high pressure, while at higher temperatures the liquid asphaltene-rich phase is heated to

drive off the solvent as vapor.[41] In all cases, the separated asphaltene-rich phase contains the *n*-alkane solvent until it is stripped off or evaporated.

1.2. Impact of Nanoaggregation on Asphaltene Phase Behavior. Several phase behavior models have been used successfully to correlate and predict asphaltene phase separation, including cubic equations of state (CEOS), the cubic plus association (CPA) equation of state, perturbed chain statistical associating fluid theory (PC-SAFT), and modified regular solution theory (MRS). Examples of phase behavior models are listed in Table 2. In these models, crude oils are characterized into a set of pseudocomponents. Depending on the model, properties such as density, molecular weight, boiling point, and/or solubility parameters are assigned to each pseudocomponent. In all these models, the molecular weight of the asphaltenes is the mean value for aggregated and nonaggregated components in solution. The properties of the nonasphaltene fraction of the oil (maltenes) are constrained by measured values from the crude oil or correlations developed from measured values from other oils. However, there are few data with which to constrain all the properties of the asphaltenes, particularly their molecular weight.

The models listed in Table 2 do not require any direct information on the elemental composition, structure, or true physical dimensions of the asphaltene molecules or nanoaggregates. Any impact of these variables is indirect through the density and the distribution of nanoaggregate molecular weight

(or segment (monomer) molecular weight and number of segments per molecule), which is driven by molecular association behavior. The average density of asphaltenes ranges from approximately 1100 to 1200 kg/m^3 depending on the source and how the asphaltenes were extracted from the oil, but there are few data on the distribution of the densities within the asphaltene fraction. Barrera et al.[46] fractionated asphaltenes extracted from a bitumen in solutions of *n*-heptane and toluene. They determined the density of each fraction from the densities of solutions of the fraction in toluene. The densities of the fractions ranged from approximately 1100 kg/m^3 for the most soluble asphaltenes to 1200 kg/m^3 for the least soluble asphaltenes. Approximately 90% of the asphaltenes had densities between 1150 and 1200 kg/m^3, suggesting that 90% of the asphaltenes were nanoaggregates with similar densities, and 10% were individual molecules.

The boiling points of the asphaltene components are extrapolated from a distillation assay. Their solubility parameters are less constrained but must be consistent with the trends within the maltene parameters and fall within the bounds set by known molecular species. However, the molecular weight distribution of the asphaltene nanoaggregates is not known, and there is no constraint on its upper end. For modeling of phase behavior, the molecular weight of the asphaltene nanoaggregates is input either as a single average nanoaggregate molecular weight or as a distribution of asphaltene molecular weights. This average or distribution can affect the phase behavior calculations in three ways:

(1) In general, the larger the molecular weight of a component is, the lower its solubility in the mixture is.

(2) Since crude oil assays are mass based, a higher molecular weight gives a lower mole fraction for that component in the mixture. The distribution of mole fractions affects the predicted phase behavior.

(3) Molecular weight is sometimes an input in the property correlations for the components in the mixture, and these properties affect the predicted phase behavior.

Figure 2a shows the effect of different average nanoaggregate molecular weights on the predicted onset and amount of precipitation from one phase behavior model for an *n*-heptane diluted bitumen. Figure 2b shows the effect of using a single average molecular weight for the asphaltenes instead of a distribution of molecular weights. The phase behavior is sensitive to both the average and the distribution of the asphaltene molecular weights. Hence, phase behavior modeling can provide some constraints on the plausible molecular weight distributions for asphaltenes. Since any errors in the input molecular weight distributions or other crude oil input properties are compensated for when the models are tuned to fit the observed phase behavior, the distributions are best considered as qualitative.

The molecular weights used in different asphaltene precipitation models (Table 2) have mean values ranging from 1000 to 3000 g/mol. The mean values differ depending on the selected model, values of other model input parameters, and crude oil. When a distribution of molecular weights is used, the maximum value for asphaltene aggregates is constrained by the solubility, giving maximum values in the range of 4000−30,000 g/mol. Of course, if the phase behavior models are not appropriate representations of asphaltene precipitation, the inferred distributions are meaningless.

Effective modeling of asphaltene phase behavior using the available equations of state can only be achieved when asphaltene aggregates are included, via tuning of molecular weight or molecular weight distribution. The molecular weights of the asphaltene fraction must exceed the molecular weights of the component molecules to fit available experimental data. While the models are amenable to incorporating detailed modeling of aggregation to obtain the detailed distribution of molecular weight, the data of Table 2 indicate that very little data are required to predict the onset of asphaltene precipitation in whole crude oils. A more representative distribution of aggregates only becomes important when modeling more detailed behavior, as illustrated in Figure 2. Hence, bulk asphaltene phase behavior supports the existence of nano-aggregates but is not very sensitive to their molecular weight distribution and provides little insight into nanoaggregation.

1.3. Asphaltene Material Properties. Another feature of asphaltene phase behavior is a glass transition in the asphaltene-rich phase. Even though the laboratory preparation of the asphaltene fraction gives a powdery solid, all asphaltene-rich phases are liquids at high enough temperature. As mentioned above, the transition temperature for Athabasca bitumen is ca. 90 °C. Below the transition temperature, asphaltene-rich materials are glassy solids. Glass transition temperatures for asphaltene materials occur over a range of temperatures, with the onset and end point dependent on their preparation and composition, and form a continuum of behavior with petroleum vacuum residues and asphalt cements. The glass transition temperature increases with the C$_5$-asphaltene content of a sample; for example, for Athabasca the onset of the glass transition increased from −47 °C for C5 maltenes to −36 °C for a sample with 50 wt % C5 asphaltenes.[47] The glass transition temperatures were much higher for four C$_7$-asphaltene samples that did not contain maltenes, in the range 120−130 °C.[48]

Asphalt cements, which normally contain both C$_5$-asphaltenes and maltenes, do not have a conventional melting point. They transition from viscoelastic solids to Newtonian liquids between 20 and 70 °C. As the asphaltene content increases, so does the temperature of this fluid transition. On the basis of the measurement of phase angle as the sample is heated, Athabasca C$_5$-asphaltenes shifted from a phase angle of 0° (viscoelastic) at 111 °C to a phase angle of 90° at 229 °C (Newtonian fluid).[47] C$_7$-Asphaltenes from various crude oils formed liquid melts at ca. 230 °C, based on observations of solid samples during heating.[48,49]

At ambient conditions, asphaltene-rich solids exhibit conchoidal fractures like other glassy solids, as observed for gilsonite minerals that contain about 80 wt % C$_5$-asphaltenes.[50] Identifying these material properties of asphaltenes is important in understanding their transport properties. Glassy solids have much lower diffusion coefficients than liquids; for example, toluene in solvents has a diffusion coefficient of the order 10^{-9} m^2/s, which decreases to 10^{-11} m^2/s in a viscous liquid like Athabasca bitumen.[51] In glassy solids, like polystyrene, the diffusion coefficient decreases to 10^{-13} m^2/s.[52] Even though the dimensions of precipitated domains of solid asphaltenes are very small, the low diffusion coefficients in the glassy phase will give very low rates of transport of the larger asphaltene components with the liquid phase. Even in the absence of any molecular aggregation, these low diffusion rates will give slow kinetics during washing or extraction once the asphaltene phase has formed.
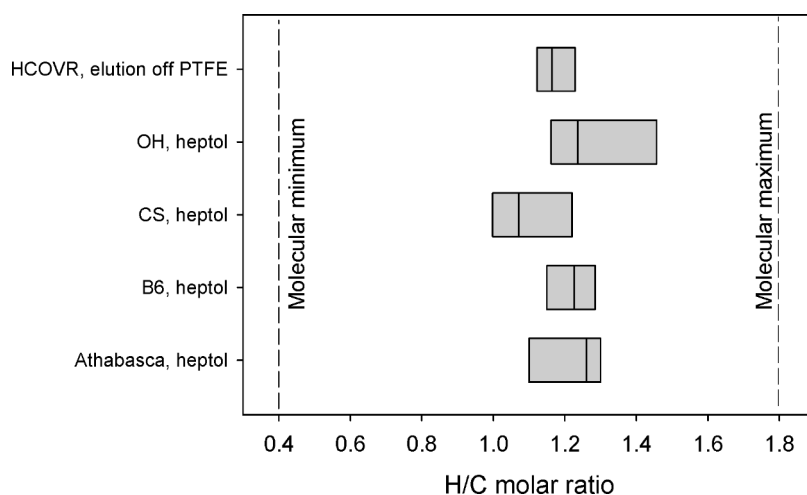
Figure 3. Range of H/C ratio from fractionation of asphaltenes in comparison to the full molecular range. Each box indicates the lowest and highest H/C ratio of separated fractions, while the line within the box indicates the mean value for the asphaltene sample. Molecular bounds are from Table 1. Data for sample HCOVR are from Rogel et al.[57] Data for OH, CS, and B6 are from Gawrys et al.[56] Data for Athabasca are from Yang et al.[5]
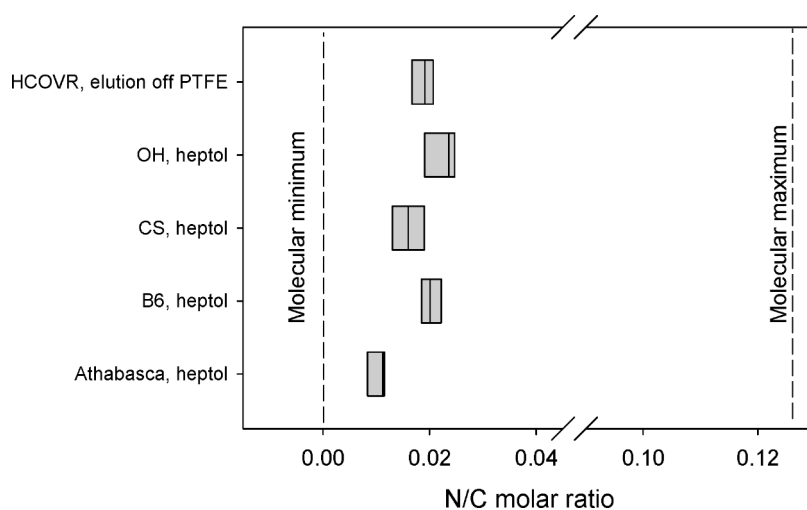

Figure 4. Range of N/C ratio from fractionation of asphaltenes in comparison to the full molecular range. Each box indicates the lowest and highest N/C ratio of separated fractions, while the line within the box indicates the mean value for the asphaltene sample. Molecular limits are from Table 1. Data for HCOVR are from Rogel et al.[57] Data for OH, CS, and B6 are from Gawrys et al.[56] Data for Athabasca are from Yang et al.[5]

Models for the rheology of asphaltene solutions suggest that the interactions of the nanoaggregates are important for viscoelastic behavior at low temperatures and for the glass transition temperature.[53−55] The solvation of the aggregates as a function of temperature appears to be significant in determining their effective hydrodynamic radius in solution. These models do not require a distribution of asphaltene aggregation, from single molecules to much larger species as detected by mass spectrometry and AFM, to represent the available viscosity data. Again, the details of nanoaggregation appear to have little impact on phase behavior, and consequently, phase behavior provides little insight on the distribution of nanoaggregate properties or composition.

2. INSIGHTS FROM SUBFRACTIONATION OF ASPHALTENES BY SOLUBILITY

The extreme molecular complexity of the asphaltene fraction has been recognized for decades, which has led to many attempts to fractionate the mixture to obtain fractions enriched in different molecular types, analogous to separation of saturates and aromatics from petroleum. As illustrated in Figure 2, the amount of asphaltene that precipitates from a solution depends on the amount of n-alkane added. For a given choice of precipitating solvent, the yield of an asphaltene-rich phase as a function of solvent composition gives information on the distribution of solubility properties within the asphaltene fraction. A number of studies have used fractional precipitation or dissolution of asphaltene samples to attempt to obtain fractions with narrower distributions of components than the initial whole sample, in order to understand the underlying molecular compositions. In some studies, the asphaltenes were fractionated into solubility cuts by precipitating a fraction of the asphaltenes in different solvents. For example, Gawrys et al.[56] separated several asphaltenes from heavy oils, and Yang et al.[5] separated Athabasca C_7 asphaltenes by adding mixtures of toluene and heptane. By successively increasing the concentration of heptane, the asphaltenes were separated into fractions of successively lower solubility. The cumulative precipitation curve in this case is similar to the data of Figure 2a, but the precipitated phase is collected at each step for characterization.

In an alternate approach, Rogel et al.[57] eluted Venezuela asphaltenes from a column packed with PTFE using successively higher concentrations of toluene in heptane. In this section, we compare the analysis of asphaltene subfractions from three studies of this type to the full range of molecular chemistry as revealed by the combination of extrographic separation and FT-ICR mass spectrometry.

The data of Figure 3 illustrate the results for the H/C ratio. The mean values for the asphaltene samples were in the range from 1.07 to 1.26. The upper and lower bounds for molecular H/C ratio are generic estimates from the data of Table 1 for petroleum asphaltenes, because the actual molecular data are not available for the four crude oils in Figure 3. The subfractions gave a wider range of H/C than the whole sample, but even the broadest range from OH asphaltenes was much narrower than the full molecular range from 0.4 to 1.8. The data of Figure 4 show the data for the N/C ratios for the same samples. Although the nitrogen compounds are significantly more polar than the hydrocarbon or sulfur compound classes, the subfractionation gave only a very narrow range of N/C in comparison to the full molecular range. On the basis of FT-ICR MS analysis, the N-containing compounds have much narrower distributions of DBE and carbon numbers than the S- and O-containing molecules.[12] They also tend to have much higher DBE values (and are closer to the PAH limit) than S- and O-containing molecules.

Separation by solvent solubility was even less effective for concentrating vanadium than for total nitrogen. For an asphaltene sample containing 1080 ppmw of vanadium, Yang et al.[5] reported a maximum concentration of only 1110 ppmw in one subfraction of Athabasca asphaltenes. Gawrys et al.[56] reported a maximum concentration of 1400 ppmw of vanadium in a subfraction of B6 asphaltenes, in comparison to a sample mean of 1100 ppmw. Much higher enrichment of vanadium is possible. For example, from Athabasca asphaltenes, McKay Rytting et al.[58] achieved a concentration of over 22,000 ppmw for a V/C ratio of 0.0064, but this level of enrichment relied on multiple chromatographic separation steps.

On the basis of the data from extrography separation and FT-ICR MS of asphaltenes,[1] the O/C ratio of individual species can be as high as 0.25 (Table 1). Few studies have reported oxygen contents of asphaltene subfractions, and even when reported, the data are likely biased high due to oxidation by air during the separations. For example, Gawrys et al.[56] reported a mean O/C value for B6 asphaltene of 0.02, but the O/C values for the Heptol subfractions were all higher than the mean, in the range from 0.021 to 0.031. The separation scheme of Kharrat,[59] using different ratios of tetrahydrofuran and hexane to fractionate asphaltenes, gave a range of O/C from 0.026 to 0.031 in seven subfractions of an Athabasca asphaltene with a mean O/C of 0.028. Wang et al.[60] used extrographic separation on silica to fractionate a Venezuelan heavy oil, giving subfractions with O/C from 0.017 to 0.056, for an initial sample mean O/C of 0.012.

All of the elemental ratios, including H/C, N/C, V/C, and O/C, give a much narrower range of compositions in the solvent solubility subfractions than the full molecular range. As illustrated in Figure 4 for N/C, the subfractions give a very narrow range of variation in comparison to the components in the mixture with the highest nitrogen content. Similarly, the selectivity of these separations for vanadium and oxygen species is insignificant in comparison to the full molecular range of composition. Two factors may contribute to the lack of selectivity of these fractionations:

(a) Phase separations in multicomponent mixtures remove a broad range of components and are not inherently selective for molecular composition. This behavior is illustrated in Figure 1, where the heavy asphaltene-rich phase can contain a significant amount of nonasphaltene material, as well as solvent components. Although the mean solubility parameters of the asphaltene subfractions vary with the solvent blends used for the separations,[57] each subfraction contains species with a broad distribution of the solubility parameter. The solubility parameter depends on multiple molecular contributions due to aromatics, alkyl chains, and cycloalkyl groups in addition to functional groups of heteroatoms such as nitrogen or oxygen. In addition, the asphaltene fraction contains molecules with more than one heteroatom.[4] A continuum of complex molecules with multiple structural features cannot be separated cleanly based on solubility.

(b) Intermolecular interactions and aggregation may effectively mask the most polar or distinctive species in the mixture, giving interactions with the solvent phase that tend to the mean of groups of molecules or the exterior of aggregated components, rather than the full range of individual components. The behavior illustrated in Figure 3, in Figure 4, and in the data for vanadium and oxygen are completely consistent with the presence of aggregates. Apart from OH asphaltenes, the H/C ratios fall in a narrow range around the sample mean. Although the nitrogen species are more polar than the hydrocarbons or sulfur species, they do not selectively appear in one or two subfractions. The hydrogen bonding oxygen species fall uniformly across the subfractions, likely because they are among the strongest contributors to aggregation.[1] If the oxygen species initiate aggregation, forming the kernel of an aggregate, the groups at the exterior of the aggregate would then determine the effective solubility parameter and give rise to a complete lack of selective separation in solvent fractionations.

Measurements of average aggregate properties showed differences between fractions in some but not all cases. All the Athabasca subfractions gave apparent molecular weights in the range of 12,000−15,000 g/mol in toluene at 50 °C and a concentration of 30 g/L.[5] Although OH asphaltene fractions showed a larger range of H/C in its subfractions (Figure 3), it gave the same range of aggregate dimension as B6,[56] with radii of gyration in 1-methylnaphthalene/methanol solution ranging from 2.5 to 7 nm for both B6 and OH asphaltenes. The radius of gyration increased with the solubility parameter of the Heptol mixture used for precipitation of each subfraction.

Although phase separation from crude oil is a defining property of the asphaltene fraction, the data for phase separation from whole crude oils and differential solvent separation of asphaltenes in solution do indicate the underlying molecular complexity. Any precipitation of asphaltene fractions, whether from crude oil using *n*-heptane or from asphaltene solutions using heptane−toluene mixtures, gives heavy precipitated phases with a very broad range of molecular components. Modeling of these processes requires only rudimentary information on distribution of molecular weight in solution and so gives very little insight on asphaltene aggregates. Conversely, detailed information on the distribution of aggregate behavior is not required for modeling beyond a distribution of molecular weights.
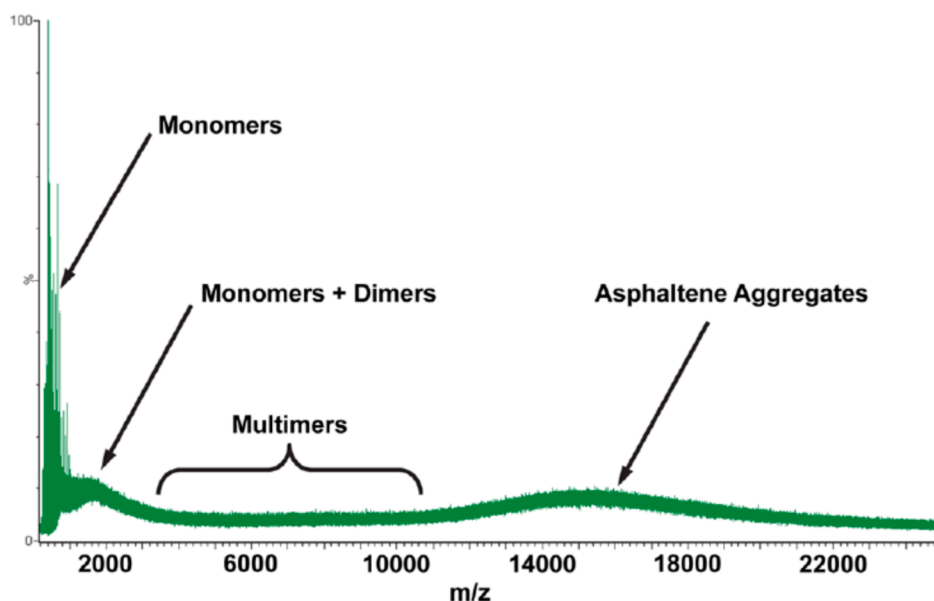
G

Figure 5. Mass spectrum for 250 μg/mL Middle Eastern heavy crude oil acquired by electrospray ionization in positive-ion mode (+ESI). Asphaltene monomer, dimer, and multimer distributions are observed, extending up to ~22 kDa, demonstrating asphaltene aggregate formation in whole crude oil at concentrations below those required for all mass analyzers. The solvent system is 50:50 toluene/methanol.[24] Reproduced with permission from ref 24. Copyright 2013, American Chemical Society.

3. INSIGHTS FROM MEASUREMENTS OF MOLECULAR WEIGHT AND SIZE DISTRIBUTIONS OF ASPHALTENE AGGREGATES

Any separated asphaltene-rich phase contains both free molecules or monomers and nanoaggregates composed of different numbers of molecules. The distribution of nano-aggregates is superimposed on the distribution of free monomer species, giving a distribution of any property of interest. This section focuses on the measurement of distributions in molecular weight and in size of the mixture of free and aggregated molecules in solution. The definition of molecular weight is unambiguous, but the definition of the dimensions of a molecule or nanoaggregate in solution is much more complex and method dependent. In this review, we define size as the effective radius in solution, determined by methods such as filtration and gel permeation that are most influenced by the hydrodynamic radius. The preceding discussion of the bulk behavior of asphaltenes in phase separations and in differential separations based on precipitation demonstrated that the diversity of molecular structure in the asphaltene fractions was not evident in the analysis of asphaltenes and asphaltene subfractions. A wide variety of techniques have been used to detect the onset of asphaltene aggregation as low as 25 mg/kg[61,62] and to determine the average size or molecular weight in crude oils, vacuum residues, or solvent solutions,[26] but most of these methods give no direct indication of the size distribution or maximum size of asphaltene aggregates.[61] Determination of the average molecular weight of aggregates cannot define the distribution, and analysis of mean molecular weights of subfractions from solvent precipitation does little to define the distribution because there is too much averaging of composition due to the nature of the phase separation, as demonstrated in the previous section of this review.

To define a distribution of nanoaggregate properties, the asphaltene mixture must be separated based on aggregate size or molecular weight; then, the abundance of each fraction must be measured. Four methods have been reported that have the

potential to provide such direct determinations: mass spectrometry, nanofiltration, sedimentation, and diffusion through pores. Finally, direct measurement of average molecular weights of asphaltenes and resins in solution at different concentrations by vapor-pressure osmometry has been used to infer the underlying distribution behavior.

3.1. Distribution of Aggregate Molecular Weights from Mass Spectrometry. McKenna et al.[24] used mass spectrometry to detect the formation of asphaltene aggregates as a function of concentration to test the hypothesis that aggregation of samples was significant at the sample concentrations typically used for analysis. As illustrated in Figure 5, the monomer distribution was overlaid by dimers, and aggregates were detected up to 22 kDa. Aggregation was largely suppressed only when the concentration was reduced to below 50 ng/mL (approximately 50 ppb by weight). This result demonstrated that aggregation may persist down to very low concentrations, biasing the results from mass spectrometry at typical sample concentrations.

This study gives proof of aggregation even at very low concentrations, but it cannot be regarded as a quantitative method for determining molecular weight distribution of asphaltenes in a solution. Although asphaltenes are not highly soluble in methanol, this study used a mixture of 50:50 methanol + toluene. The apparent maximum in the distribution of aggregates was dependent on the instrument used and the details of operation, with a peak at m/z of 7 kDa on one instrument and 15 kDa on another, at the same sample concentration. The efficiency of ionization over the entire range of mass could not be verified to determine whether the distribution of m/z in Figure 5 represented the true distribution of molecular weight in solution or whether detection was biased toward large aggregates or monomer molecules.

Rather than beginning with solutions of asphaltenes, Wu et al.[63] used laser desorption of an asphaltene film to determine a distribution of molecular weights. A unimodal distribution of asphaltene molecules, with average molecular weight of 580 Da,

gave unimodal and multimodal distributions of ions of up to 8000 Da. The distribution of m/z of the ions depended on both the laser power and the thickness of the film. The test compound coronene gave a spectrum composed of fragmentation ions of $m/z < 300$, ionized coronene at 300 Da, and a distribution of multimers, from dimers up to at least 10 molecules, with an exponential decrease in abundance with m/z. The m/z distribution was inferred to be the signal from multimers of asphaltene monomers, as an instrumental artifact, overlaid by the signal of "true" asphaltene aggregates. On the basis of this interpretation of the spectrum, the mean aggregation number was inferred to be 6−8 molecules. This interpretation, based exclusively on a mode in the ion distribution at 400−500 Da, excluded the possible existence of smaller nanoaggregates of 2−4 molecules or larger aggregates.

Although coronene gives no significant aggregation in solvents such as toluene, the SALDI-MS method generated significant aggregate signals from a solid film of material. Consequently, most of the ions detected were an artifact of the instrument and have no relationship to aggregation of asphaltene species in crude oil or solvent solutions. No attempt was made to calibrate the response of the instrument using a model mixture of aggregates, of defined mass and composition, with a monomer compound such as coronene. Without such a calibration, the method is at best qualitative. Consequently, we conclude that neither solution-phase mass spectrometry[24] nor laser-desorption mass spectrometry[63] methods have been calibrated to give quantitative measurements of distributions of molecular weight of asphaltene aggregates.

3.2. Size of Aggregates from Nanofiltration. The stability of asphaltene nanoaggregates in solution enables physical separations based on size. For example, Zhao and Shaw[22] used nanofiltration of whole crude oil at 200 °C to retain an asphaltene-rich liquid. The concentration of asphaltenes in the permeate showed that the most abundant aggregates in Athabasca bitumen were 10−20 nm in size, while Maya crude oil gave a maximum at 5−10 nm (from data of Figure 6). The maximum size of aggregates in Maya was between 50 and 100 nm, while the maximum size in Athabasca could not be
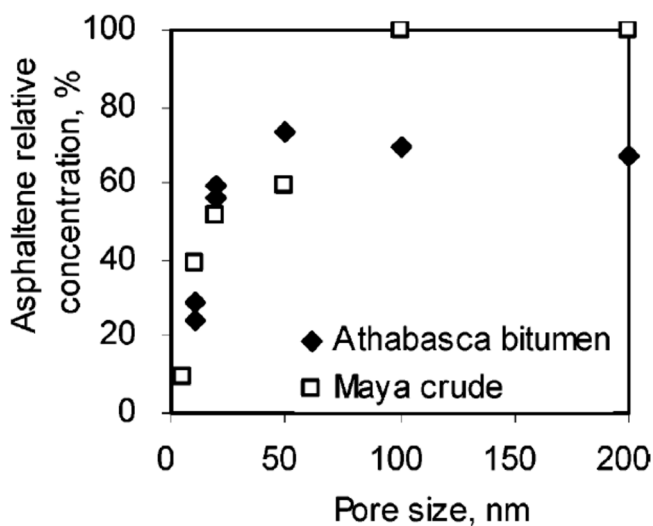
determined due to interference with fine clay material from the hot-water extraction process. The aggregate sizes determined by this method were likely a maximum estimate, due to changes in the diameters of pores in the nanofilter due to adsorption of asphaltenes.

Marques and co-workers used cross-flow filtration to separate C$_7$-asphaltenes in a toluene solution into two fractions.[64,65] A membrane with a nominal 20 kDa cutoff was used for the separation, and the solution was recirculated until asphaltene stopped passing through the membrane. The asphaltene fractions were characterized by GPC and SAXS, as shown in Table 3.

The nanoaggregate radii from pore sizes in Figure 6 are 2 to 3 times smaller than the radii of gyration in Table 3, based on the mean size of the smallest 20% of the distribution curve. Yarranton et al.[26] reported a similar discrepancy for mean size of whole asphaltenes between pore dimensions in filtration and diffusion measurements and radius of gyration from SAXS.

3.3. Molecular Weights from Sedimentation Fractions. Centrifuge studies from 1957 onward showed the presence of colloidal material in crude oil that could be removed as sediment, taking most of the metals and asphaltenes out of the crude oil, as well as significantly reducing the dark coloration of the oil[21,66] Barre et al. used ultracentrifugation to recover three subfractions with a range of apparent molecular weights from 8×10^3 to 7×10^5 g/mol, based on GPC analysis with polystyrene standards for calibration.[67] SAXS analysis of the fractions showed average radii of gyration ranging from 6 to 16 nm but did not report the yields of the fractions to enable the construction of a distribution of apparent molecular weight or size.

Mostowfi et al. collected sediments as a function of concentration of asphaltenes in toluene but did not attempt to collect subfractions to construct a distribution curve.[68] Gray and Yarranton[61] showed that these data could be modeled using a distribution of molecular weight from a stepwise-aggregation model[69,70] and suggested that transient data from ultra-centrifugation could be used to investigate aggregate size distributions. All the studies with ultracentrifugation show that a significant mass fraction of the asphaltenes are present as stable aggregates in solution.

In some reservoirs with a significant vertical oil column, the asphaltene concentration in the oil increases with depth. Composition gradients can be modeled as a balance between diffusion and settling or by introducing a gravity term into a phase behavior model. Zuo et al.[71] adapted the latter approach with a regular solution model to match compositional gradients in several reservoirs. Compositional gradients in reservoirs were determined by optical density or direct measurement of asphaltene content and were fitted using an asphaltene density of ca. 1200 kg/m^3 and tuned molecular weights of ca. 750 g/mol for molecules, 3000 g/mol for nanoaggregates, and 25,000 g/mol for clusters of nanoaggregates.[72] In most cases, a single molecular weight for the asphaltenes was sufficient to fit the data, although one example was fitted with a mixture of 80% clusters with 20% nanoaggregates. Rogel et al.[73] followed a similar approach and examined asphaltenes from two reservoirs. They found that the asphaltene gradients were consistent with average molecular weights from 1200 to 3000 g/mol for nanoaggregates. Compositional gradients were also modeled using the PC-SAFT equation of state using a single asphaltene fraction with a partial molar volume of 1932 cm^3.[74]

Although sedimentation in a reservoir could give a distribution of aggregate size as a function of depth, modeling

Figure 6. Asphaltene concentration in the permeate relative to the whole crude oil, as a function of the pore size of the nanofilter. Separation at 200 °C used whole crude oils.[22] Reproduced with permission from ref 22. Copyright 2006, American Chemical Society.

Table 3. Fractions of Asphaltene Prepared by Cross-Flow Filtration Using a Membrane with a 20 kDa Cutoff[65]

Fraction	Yield of fraction (wt %)	M_w by GPC, polystyrene standard (g/mol)	Radius of gyration by SAXS (nm)
Initial	100	7027	11.6
Retentate, high molecular weight	78	9038	15.8
Filtrate, low molecular weight	22	3637	3.3

with a single average value appears to be sufficient to fit the limited data available. Although aggregates exchange components only slowly with solution species, the geological time scales for development of asphaltene gradients would likely allow for considerable equilibration.

3.4. Size Distribution from Diffusion of Aggregates through Pores. One method for examining the distribution of sizes of molecules and nanoaggregates in solution is gel-permeation chromatography (GPC). When applied to polymers, which are monodisperse in chemical properties and distributed mainly in molecular weight, GPC gives direct measurement of a distribution of molecular size based on the diffusion of molecules into the pores of the gel packing. In a polydisperse material like asphaltenes, separation is by a combination of diffusion of both molecules and aggregates in the pores of the chromatography packing and adsorption—desorption interactions with the gel material. Although solvents such as tetrahydrofuran (THF) are commonly used in GPC to minimize adsorption, with asphaltenes these interactions are not suppressed completely, and a portion of the asphaltene sample will elute after the smallest component of the mixture, which is the solvent.[75] Although molecular weights from GPC have been reported based on use of polystyrene oligomers as calibration standards, the current view is that such calibrations are not meaningful for asphaltenes. The value of GPC is to give qualitative information on changes in aggregate distribution after separations and reactions[76] and defining the contribution of different molecular species to the aggregation behavior.[77]

The data of Figure 7 show the distributions of vanadium, nickel, and sulfur in the residue fractions of a crude oil as determined from a combination of GPC with inductively coupled plasma with high-resolution mass spectrometry detection.[78] The size ranges are indicated qualitatively, with HMW as high molecular weight, MMW as medium molecular weight, and LMW as low molecular weights. The LMW fraction was molecular species and small aggregates from both the asphaltene and maltene fractions, while the HMW and MMW fractions were nanoaggregates from the asphaltenes. The sulfur was more uniformly distributed, consistent with its abundance over the entire range of crude oil fractions.

The qualitative information on different sizes of nanoaggregates from GPC has been used in several studies to explore the kinetics of association and dissociation.[6,76] For example, the data of Figure 8 show the significant shift in the distribution of vanadium in THF solution to the HMW fraction with time. These data illustrate the slow rearrangement of aggregates at ambient temperature, even at high dilution in solvent. These long-term changes in solution could be driven by oxidation of asphaltenes in solution, as demonstrated by Yarranton et al.,[28] rather than slow kinetics of molecular aggregation-disaggregation.

The penetration of asphaltenes into catalyst materials is extremely important in refinery processes such as catalytic hydroprocessing, because the large molecules and nanoaggregates diffuse more slowly than the lighter fractions of crude oil. Penetration of asphaltenes from solution into catalyst
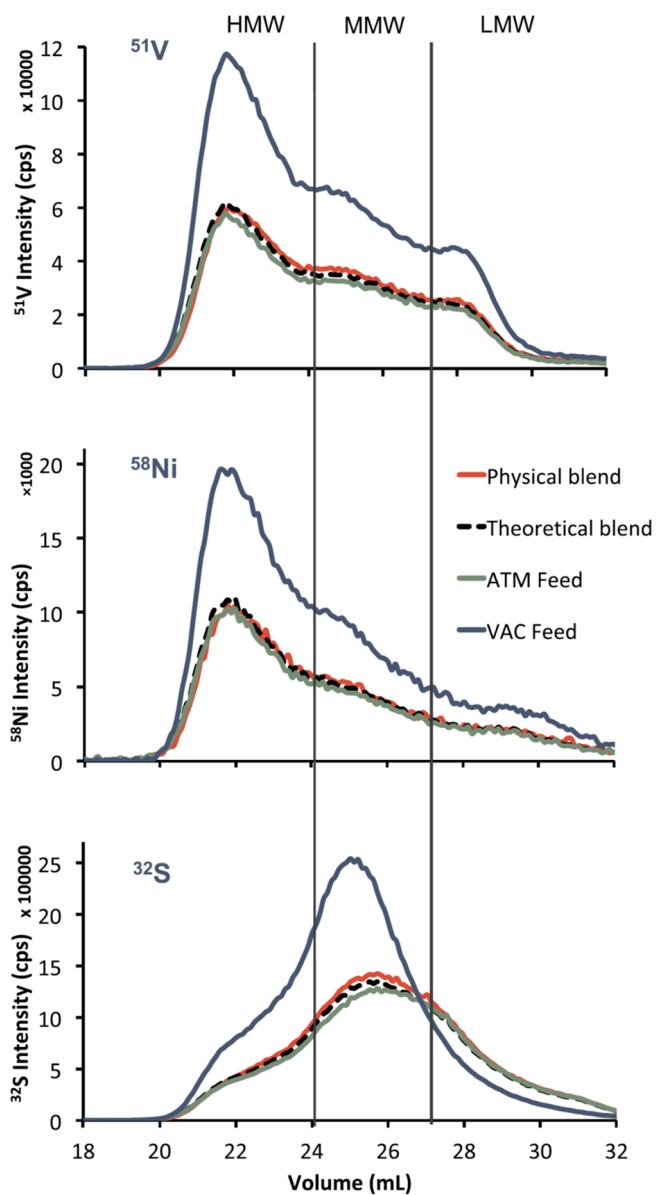

Figure 7. GPC ICP-HR-MS chromatograms of the V, Ni, and S species in an atmospheric residue feedstock (ATM, green line), vacuum residue (VAC, blue line), blend of 93 vol % ATM, and 7% VAC (physical blend, red line) and theoretically reconstructed blend of 93 vol % ATM and 7 vol % VAC (black dashed).[78] Reprinted from ref 79. Copyright 2020, with permission from Elsevier.

pellets has been measured at up to 250 °C without reaction, but the complex combination of adsorption and diffusion with potential dissociation of asphaltene nanoaggregates prevents any determination of the distribution of molecular or nanoaggregate size.[79] Although significant dissociation of nanoaggregates might be expected at temperatures of 250 °C, the comparison of the penetration of low- and high-molecular weight fractions and the size of the asphaltenes remaining in solution after uptake by
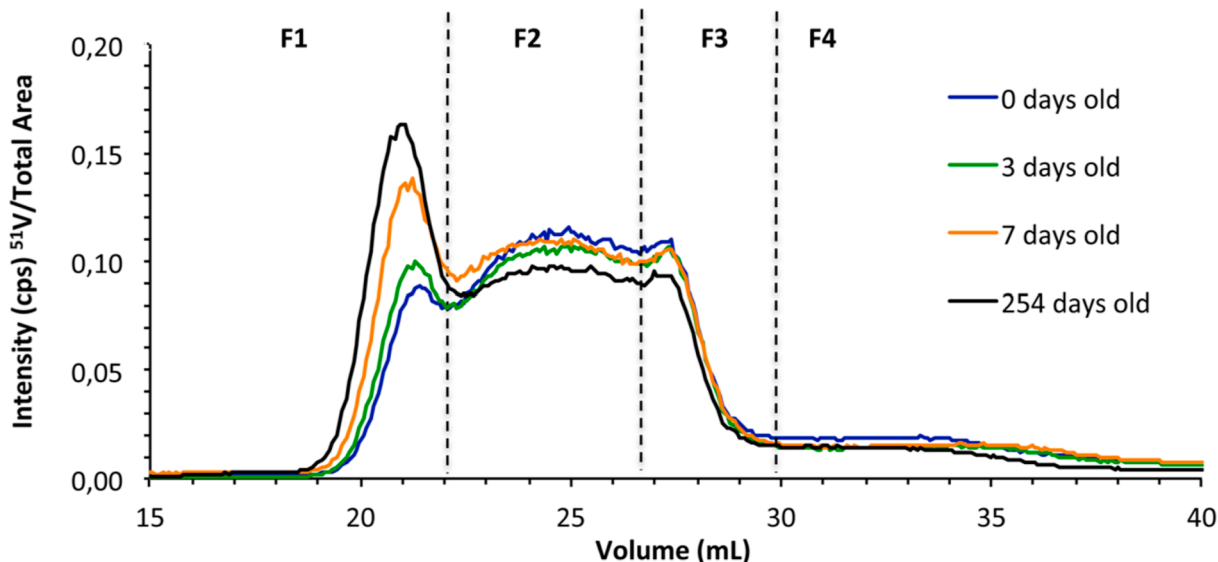
Figure 8. Evolution over time of the GPC ICP-HR-MS data normalized with respect to their total area obtained for vanadium aggregates of the vacuum residue fraction dissolved in solutions of stabilized THF.[76] F1 fraction is HMW. F2 fraction is MMW. F3 fraction is LMW. Reproduced with permission from ref [77]. Copyright 2016, American Chemical Society.

catalyst pellets both indicated significant persistence of nano-aggregates. Separation and characterization of the most persistent nanoaggregates, after hydroprocessing, would give insight into the composition and behavior of this important subfraction of the asphaltenes.

Similar to diffusion through porous catalyst materials, the rate of diffusion through membranes gives an indication of the size of the most abundant aggregate sizes in dilute solutions, which were in the range of 5−10 nm for Athabasca C_7-asphaltenes based on diffusion through nanoporous membranes.[23] Baltus and Anderson[80] combined GPC analysis with pore-diffusion measurements to estimate the distribution of size of the asphaltenes. Using the Stokes−Einstein equation to estimate the hydrodynamic diameter of GPC subfractions asphaltenes in THF at 25 °C, they determined a size range from 5 to 30 nm, with a mode at 6−9 nm. This range was narrower than the results illustrated in Figure 6 from nanofiltration.

3.5. Asphaltene Molecular Weight Distributions from VPO. The average molecular weights of asphaltenes in toluene solutions can be measured for concentrations from 1 to 100 g/L by vapor-pressure osmometry (VPO). As illustrated in Figure 9, the average molecular weight of asphaltenes increases with concentration due to aggregation, in contrast to the resins which show no concentration dependence. Mixtures of asphaltenes and resins show an intermediate response, with less aggregation and less sensitivity to concentration. These trends were successfully modeled as competition between asphaltenes and resins for sites on growing aggregates, with the asphaltenes propagating the growth of the aggregate and the resins terminating it.[70] This simple model requires the molecular weights of the asphaltene monomers as propagators (M_p), the resins as terminators (M_t), the initial ratio of propagators to terminators in the solution (T/P), and the association constant for addition of a propagator or terminator to an aggregate (K). The model is effective in giving a consistent representation of the data from VPO as a function of concentration and composition.

The molecular weight distribution of nanoaggregates from this VPO-based model approximately follows a gamma distribution, as illustrated in Figure 10, in comparison to an
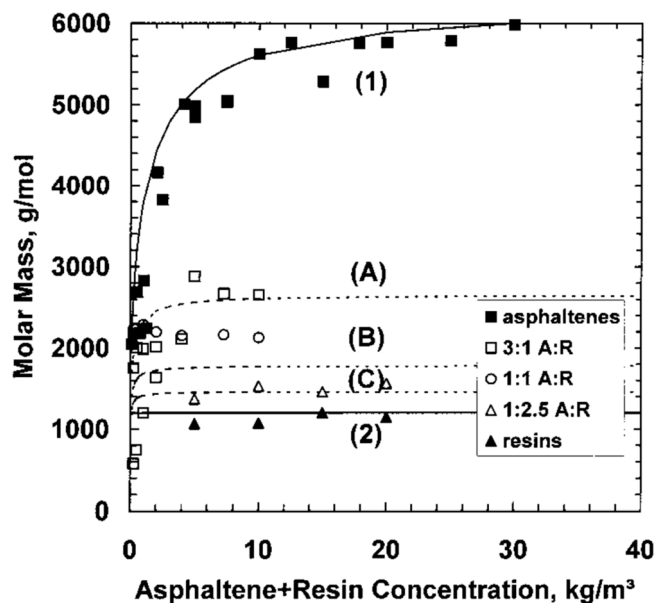

Figure 9. Molar masses of Athabasca C5-asphaltenes and resins in toluene at 50 °C as determined by vapor-pressure osmometry.[70] For mixtures, A:R denotes the mass ratio of asphaltenes to resins. Model curve fits with M_p = 1800 g/mol, M_t = 800 g/mol, and K = 130,000: (1) $(T/P)^0$ = 0.33 and (2) $(T/P)^0$ = 4.5. Model predictions: (A) $(T/P)^0$ = 0.97, (B) $(T/P)^0$ = 1.84, and (C) $(T/P)^0$ = 2.73. Reproduced with permission from ref [71]. Copyright 2001, American Chemical Society.

estimated distribution of monomer molecular weights from 400 to 1500 g/mol. The models based on VPO data suggest that nanoaggregate molecular weights range from approximately 1600 g/mol (dimers) to 40,000 g/mol (approximately 50 molecules per aggregate) with much lower abundance of large aggregates. As a result of this observation, gamma distributions of nanoaggregate molecular weights have been successfully used in modeling and predicting asphaltene phase behavior, including high- and low-temperature phase separations (Figure 1), yields of precipitate as a function of heptane concentration (Figure 2), precipitation by different n-alkanes,[81] and composition of
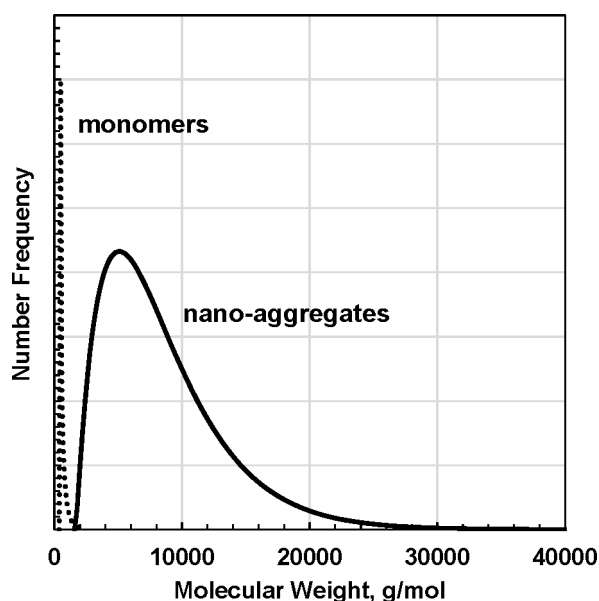
Figure 10. Comparison of approximate asphaltene monomer and nanoaggregate molecular weight distributions based on VPO measurements.

asphaltene-rich phases.[34] While the mean value of the distribution curve is determined experimentally and the lower bound is constrained by the asphaltene monomers, the upper bound in Figure 10 is not directly based on experiments. Different experimental approaches to measuring distributions of nanoaggregate properties are discussed in later sections of this review.

4. INSIGHTS FROM SURFACE PROPERTIES OF NANOAGGREGATES

4.1. Stabilization of Oil−Water Emulsions. Asphaltenes can stabilize emulsions by adsorbing at water/oil interfaces.[82−84] They can adsorb both as individual molecules and as nanoaggregates,[85] initially giving a rapid decrease in interfacial tension, followed by a period of much slower decrease.[86,87] The initial rapid decrease is consistent with diffusion-controlled attachment to the interface, while the subsequent slow changes in interfacial tension are consistent with an interfacial barrier or molecular rearrangement at the interface. The elasticity of these interfaces increases over time consistent with molecular rearrangement.[88−90] The increase in elasticity occurs more rapidly and is more extensive in poor solvents below the onset of asphaltene precipitation. Given time, asphaltenes form irreversibly adsorbed films.[91] The irreversible films form more rapidly in poorer solvents and at higher asphaltene concentrations. These films can only be partially compressed before the interface buckles.[88,92] They are effective at stabilizing emulsions through their resistance to compression during coalescence[93] and inhibition of drainage.[83] These characteristics of asphaltene interfacial films are similar to behaviors of some globular proteins, which may either retain a fixed dimension at the interface or undergo partial unfolding and rearrangement.[94]

Rigid interfacial asphaltene films are formed by a relatively small nonrepresentative fraction of the asphaltenes. Yang et al.[95] and Qiao et al.[96] found that only a small fraction (<2 wt %) of the asphaltenes in their study contributed to the formation of rigid interfacial films and stable emulsions. Rocha et al.[97] found that the fraction of asphaltenes capable of stabilizing emulsions was

significantly different in asphaltenes from different sources, ranging from a few wt % to over half of the asphaltenes. In all cases, only a portion of the asphaltenes could form interfacial films that stabilized emulsions. Several authors have established that the asphaltenes that form rigid films correspond to the asphaltenes which are least soluble in heptane−toluene blends and are also the most aggregated.[96−99] These asphaltenes are enriched in oxygen, sulfur, and metal functional groups.[96,100]

These observations suggest that the surface properties of asphaltene aggregates are highly heterogeneous and that a subfraction of aggregates adsorb strongly to oil−water interfaces. While nonaggregated polar molecules acting as conventional surfactants in solution can form interfacial films, the gradual formation of a rigid film over time is more consistent with aggregates cross-linking at the interface to form a rigid film. The polarity which contributes to formation of aggregates in solution[1] in turn would contribute to film rigidity.

Figure 11 presents an interpretation of rigid asphaltene film formation based on studies of asphaltene-stabilized emul-
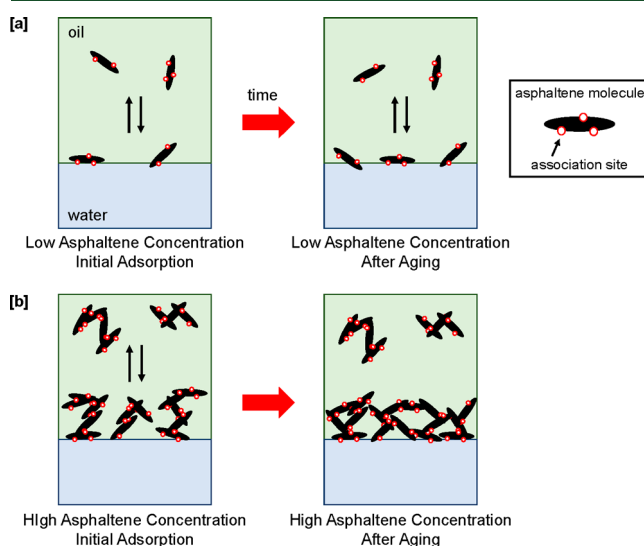

Figure 11. Hypothesized dynamic behavior of asphaltenes at the water−oil interface: (a) At low asphaltene concentrations, the asphaltenes adsorb reversibly as molecules and the film remains irreversibly adsorbed over time. (b) At high asphaltene concentrations, the asphaltenes initially adsorb reversibly as nanoaggregates which rearrange and become irreversibly adsorbed over time.

sions.[96−99] At low concentrations, nonaggregated molecules mainly adsorb at the interface. There is little or no cross-linking, and the film is reversibly adsorbed with low elasticity and little ability to stabilize emulsions. At higher concentrations, nano-aggregates adsorb at the interface. Initially, there is no cross-linking, and the film is reversibly adsorbed. Over time, the nanoaggregates rearrange into a two-dimensional matrix of molecules linked together by the same forces that drive nanoaggregation and are held at the interface with multiple attachments collectively and perhaps even individually. The lateral interactions and multiple attachments lead to irreversible adsorption. These irreversibly adsorbed films resist drainage and resist compression giving mechanical stability to emulsions. They possibly thicken under compression giving steric stability to emulsions. The dynamic behavior of the nanoaggregates to rearrange into an irreversibly adsorbed film is a key factor determining the film properties and emulsion stability.

Table 4. Ion Abundances (%) for GPC ³²S ICP-MS Chromatograms for Whole PetroPhase 2017 Asphaltenes and Their Acetone, Hep/Tol, and Tol/THF/MeOH Extrography Fractions[102]

Sample	prior to HMW[a] (%)	HMW (%)	MMW (%)	LMW (%)	tailing (%)
whole PetroPhase 2017 asphaltenes	1.11	64.64	25.52	6.12	2.61
acetone fraction	0.07	23.07	63.16	12.13	1.57
Hep/Tol fraction	3.09	65.78	20.70	5.86	4.57
Tol/THF/MeOH fraction	1.27	68.23	20.24	6.41	3.85

[a]Fraction eluted before the established molecular weight ranges. Material can elute before the defined MW ranges.

4.2. Adsorption to Solid Surfaces. The asphaltene fraction of crude oil exhibits strong adsorption to solid surfaces, such as silica, kaolin, and metals. Although the surface concentration often appears to follow a Langmuir isotherm, almost none of the published studies verify that desorption occurs.[101] Over the normal time scale for laboratory studies, the rates of desorption are so slow that the adsorption is both irreversible and highly nonselective for subfractions of asphaltene nanoaggregates. Consequently, the rate and extent of adsorption to solids is insensitive to any distribution of nanoaggregate properties.

The extrography studies of asphaltene desorption from silica gel demonstrate that the adsorption−desorption process can be selective for molecular separations[12] and selective for nano-aggregate properties.[102] Achieving the selective separation and almost complete recovery of the asphaltenes from the solid surface requires use of very low mass loadings and exhaustive solvent extraction over many days in the absence of oxygen. The most weakly adsorbed fraction, removed in acetone, is most enriched in "island" molecular structures for a given asphaltene sample.[12] GPC analysis of the extrographic fractions reveals that the acetone fraction is also the most deficient in HMW nanoaggregates (Table 3) and is dominated by MMW and LMW subfractions relative to the other subfractions and relative to the whole sample.

These data demonstrate that the most easily desorbed material has both the lowest tendency to aggregate and the highest concentration of island molecular structures, suggesting that this motif is not responsible for the largest most stable nanoaggregates. These data do not discriminate whether the acetone fraction desorbed as individual molecules, which then aggregated weakly in solution, or whether a subfraction of nanoaggregates was more easily desorbed than the whole sample. Conversely, the most strongly held fraction from extraction with toluene/THF/MeOH gave the highest fraction of HWM nanoaggregates in comparison to the other subfractions, but the desorption process could remove either molecules or nanoaggregates from the silica gel.

Atomic force microscopy (AFM) has been used to measure dimensions and force interactions for asphaltenes deposited on a range of surfaces. Adsorption from asphaltene solutions normally gives complete surface coverage by a film of material, but two approaches have been used to image individual nanoaggregates on surfaces. The first approach is to expose the solid substrate to a dilute solution of asphaltenes in toluene, then rinse and dry the sample for imaging.[103,104] The second is to expose the substrate to a crude oil, then remove residual liquid portions of the adsorbed asphaltene film by washing with toluene.[105] Deposition from dilute solutions onto mica gave aggregates of height from 1.1 to 4.4 nm depending on the source crude oil, with average lateral dimensions of 16−41 nm. The measurement of lateral dimensions is compromised by the large radius of curvature of the AFM tip relative to such small surface

features.[103] The dimensions of nanoaggregates in asphaltenes from a Middle Eastern crude oil depended strongly on the hydrophobicity of the surface.[103] Spherical nanoaggregates 3−4 nm thick were observed on mica, while larger irregular features were observed on calcite (2−6 nm) and silica (2−7 nm). The most hydrophobic surface, pyrolytic graphite, gave disc-shaped domains in the range 1−3 nm. The changing dimensions of the nanoaggregates depending on surface interactions suggested rearrangement of the component molecules depending on the force interactions with the surface. Washing of crude oil from a mica surface gave asphaltene domains that were much larger, ranging from 1 to 100 nm in height in a log-normal distribution with a mode of 10 nm.[105] Such large nanoaggregates were likely due to surface clusters of smaller species, which was confirmed by the significant reduction in size observed upon addition of dodecylbenzenesulfonic acid, a well-known dispersant of asphaltenes in crude oil. Together, these studies indicate that AFM analysis of asphaltenes on surfaces is a useful probe of surface attachment and the influence of forces between the surface and the attached nanoaggregates. These surface interactions in the absence of a liquid medium and the limited lateral resolution make AFM less useful for exploring the size distribution of nanoaggregates in solution and in crude oils.

5. INSIGHTS FROM PROCESSING OF ASPHALTENES IN VACUUM RESIDUES AND BITUMENS

The chemical alterations in asphaltene fractions during refining and upgrading can alter the structure and distribution of the constituent molecules and thereby alter the nanoaggregation behavior. When the chemical reactions are well understood, these shifts in molecular structure give insights into the factors that drive nanoaggregate formation. In this section, we focus on the impact of conversion under hydrogen-rich conditions in the presence of metal sulfide catalysts at temperatures of 350−450 °C on the aggregation of asphaltenes. At the lower end of this temperature range, catalytic reactions remove sulfur, nitrogen, oxygen, and metals (V and Ni) from the asphaltenes and hydrogenate some aromatic rings. Above ca. 390 °C, thermal breakage of carbon−carbon bonds becomes a significant factor, but the action of the catalyst in a hydrogen-rich environment prevents addition reactions.[106−109] Catalytic hydrogenation gives, therefore, molecular simplification that can include removal of heteroatoms (O, S, N, V, Ni, Fe), side chains, and bridged groups depending on the temperature and extent of reaction.

The persistence of nanoaggregation at refinery processing conditions would have profound impacts on the reactions of asphaltene components. Free radical species that form within nanoaggregates due to thermal reactions would be restricted in their ability to react with the bulk liquid phase. Nanoaggregates would diffuse much more slowly through porous catalyst supports, and coordination of aggregated molecules with active sites in heterogeneous catalysts would be much slower than with

Table 5. Average Molecular Weight (10 g/L Asphaltenes in Toluene at 50°C), Average Density, and Elemental Analysis of Whole Asphaltenes Hydroconverted Oils[69]

Sample	Conversion of residue (%)	Asphaltene MW (g/mol)	Density (kg/m³)	H/C	S/C	N/C
WC-SR-A3 (Feed)	0	4900	1120	1.134	0.030	0.010
WC-SR-HC56	56	2100	1180	0.938	0.005	0.009
WC-SR-HC70	70	1500	1250	0.831	0.013	0.015
WC-SR-HC80	80	900	1250	0.786	0.014	0.018

molecules in free solution, reducing the rates of reaction. Data from nanofiltration to remove asphaltenes from bitumen at 200 °C,[22] small-angle-X-ray scattering (SAXS) at 240 °C,[54] and diffusion and adsorption on catalyst pellets at 250 °C[110] show that significant concentrations of nanoaggregates persist at surprisingly high temperatures.

5.1. VPO of Feed and Product Asphaltenes. Average molecular weights of asphaltenes before and after catalytic hydroconversion at 400–430 °C were determined by vapor-pressure osmometry (VPO).[69] The molecular weight distribution was determined by modeling the VPO data over a range of concentrations using a linear-association model[70] and used to fit the observed precipitation curves of the asphaltenes in toluene–heptane solutions.

Catalytic hydroconversion, giving both removal of hetero-atoms and breakage of C–C bonds, reduced the molecular weights of asphaltene solutions and shifted the composition as indicated in Table 4. The apparent molecular weights of the product asphaltenes indicated much less aggregation than the feed sample, even though they were significantly more aromatic based on the decrease in the H/C ratio.

The model fit of the molecular weight of the asphaltenes using VPO data for concentrations from 1 to 60 g/L showed that the molecular weight of the aggregating asphaltenes, or "propagators", dropped from 2000 g/mol in the feed to 650 g/mol after 80% conversion of the vacuum residue (Table 5). The interaction of the product asphaltenes was much weaker, with a reduction in the association constant K from 13,000 in the feed to 7500 at 70%–80% conversion of vacuum residue. The fraction of asphaltenes that did not associate at all to form aggregates, designated as "neutrals", increased from 0.06 to 0.23.

The data of Figure 12 illustrate the model results for the molecular weight distribution, showing a shift from a feed population dominated by aggregates of 2000–20 000 g/mol in the feed, comprising 3–30 molecules on average, to a population dominated by monomers and dimers in the processed product. Aggregation in toluene is dramatically reduced, even though both the feed and the product asphaltenes were recovered by the same phase separation process. This observation emphasizes the conclusion from in Section 1 that significant aggregation is not a prerequisite for phase separation of asphaltenes. Catalytic hydroconversion gives multiple reactions[111,112] that drive important changes in molecular properties that can contribute to this reduction in aggregation:

(1) The linkages between aromatic groups are broken by thermal reactions, giving the release of smaller aromatics from the asphaltene fraction to the distillates.[6,107,113,114]

(2) Side chains on aromatic groups are shortened or removed by thermal reactions.[115]

(3) Oxygen-bearing groups are thermally decarbonylated or catalytically hydrogenated.[116,117]

(4) Vanadium and nickel are removed, and porphyrins are converted to hydrogenated intermediates and fragments.[62,118,119]
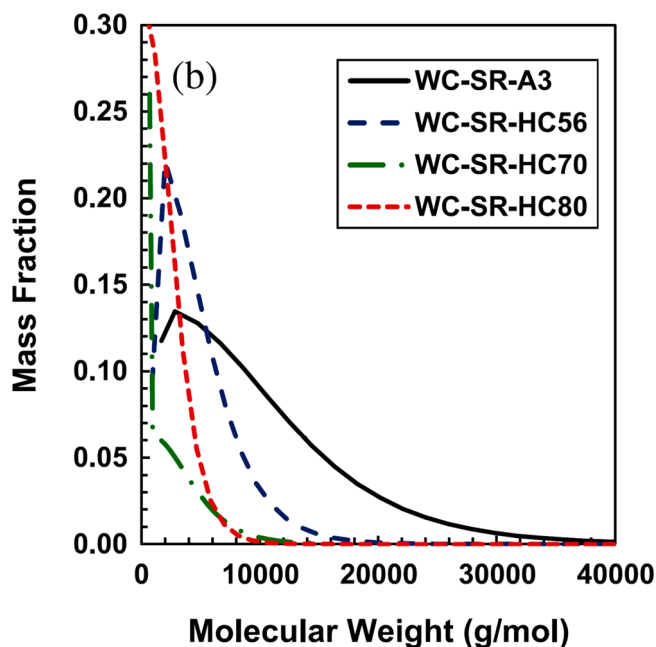

Figure 12. Modeled distribution of molecular weights of asphaltene aggregates Athabasca asphaltenes before treatment (WR-SR-A3) and after hydroconversion from 56% to 80% conversion of vacuum residue (WR-SR-HC56, WR-SR-HC70, WR-SR-HC80).[69] Reprinted from ref 70. Copyright 2016, with permission from Elsevier.

(5) Aromatic rings are partly hydrogenated, giving napthenoaromatic groups.[120,121]

Taken together, these reactions will drive a feed of Athabasca asphaltenes from a diverse mixture rich in archipelago structure and polar functional groups toward a much simpler assemblage of large aromatics and partly hydrogenated aromatics with short side chains.

5.2. GPC Studies of Feed and Product Asphaltenes. GPC of asphaltenes before and after catalytic hydroconversion gives qualitative data on shifts in aggregation behavior. Merdrignac et al.[75] examined the behavior of asphaltenes from vacuum residue from fixed-bed catalytic hydroprocessing at 380 °C and from ebullated-bed hydroconversion at 427 °C. At the lower temperature, the asphaltenes were subjected only to catalytic reactions, removing sulfur, oxygen, and vanadium giving low conversion of the vacuum residue fraction up to 23%. At the higher temperature, carbon–carbon bond breakage was significant giving high conversion of the vacuum residue fraction up to 88%. As illustrated in Figure 13, the asphaltene conversion in both cases was high, but the aggregation behaviors of the remaining asphaltenes were significantly different. At 380 °C, the extent of aggregation relative to the feed asphaltenes was only slightly reduced, despite the removal of over half of the sulfur and up to 80% of the metals. In contrast, at 427 °C, the remaining asphaltenes had only 4% of the molecular weight of the feed even at comparable conversion. At this temperature,
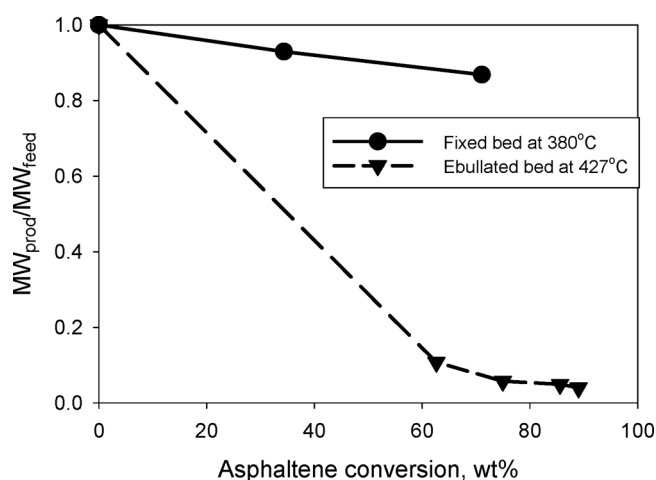
Figure 13. Average molecular weight of asphaltenes in products after catalytic hydroprocessing as a function of asphaltene conversion, relative to feed molecular weight.[75,122] Apparent molecular weights were determined from GPC data using polystyrene standards.

extensive removal of pendant aromatic and alkyl groups would occur by thermal cracking, based on the studies by Rueda-Velasquez et al.,[107] giving an increase in aromatic carbon content from 53% to 85% and dramatically reduced aggregation. This trend is the same as indicated in the work of Powers et al.,[69] who reported a significant decrease in the H/C ratio to indicate higher aromatic carbon content and a significant decrease in apparent molecular weight (Table 4).

Barbier et al.[119] used GPC ICP-MS to follow vanadium compounds during catalytic hydrotreating at 370 °C using reconstituted VR, prepared by mixing the low- and high-molecular weight fractions obtained by cross-flow ultrafiltration. They concluded that efficiency of the hydroconversion reactions is strongly linked to the molecular weight of the aggregated asphaltene present in the feed. The material in the high molecular weight fraction was much less converted.

Tracking the distribution of key elements in large aggregates during hydroprocessing provides additional insight into the aggregation behavior. Garcia-Montoto et al.[78] used ICP-HR-MS to determine vanadium, nickel, and sulfur in the GPC chromatograms of products of hydroprocessing up to 385 °C. With insignificant thermal cracking, the catalytic hydrogenation converted only 36% of the vacuum residue, but the conversion of asphaltenes was much higher at 81%. Removal of sulfur and vanadium from the vacuum residue was also high, at 93% and 92%, respectively. The distribution of the surviving V, Ni, and S by aggregation was, however, very surprising. As illustrated in Figure 14, the remaining V and Ni were almost exclusively detected in the HMW fraction. The components that gave MMW and LMW aggregates had been almost completely removed. This observation has two possible explanations: (1) The molecular species most resistant to catalytic reaction also nanoaggregate very strongly under GPC conditions so that the two behaviors are correlated. (2) Nanoaggregation of V and Ni species persists at reactor temperatures and cause the low rate of conversion of the most strongly aggregated species. The survival of nanoaggregates at 385 °C is not proven, as discussed earlier in this section. Studies of crude oils and asphaltene solutions using small-angle X-ray and neutron scattering show that nano-aggregation diminishes with temperature in the range of 100–400 °C.[54,123,124] Further studies are required to define the
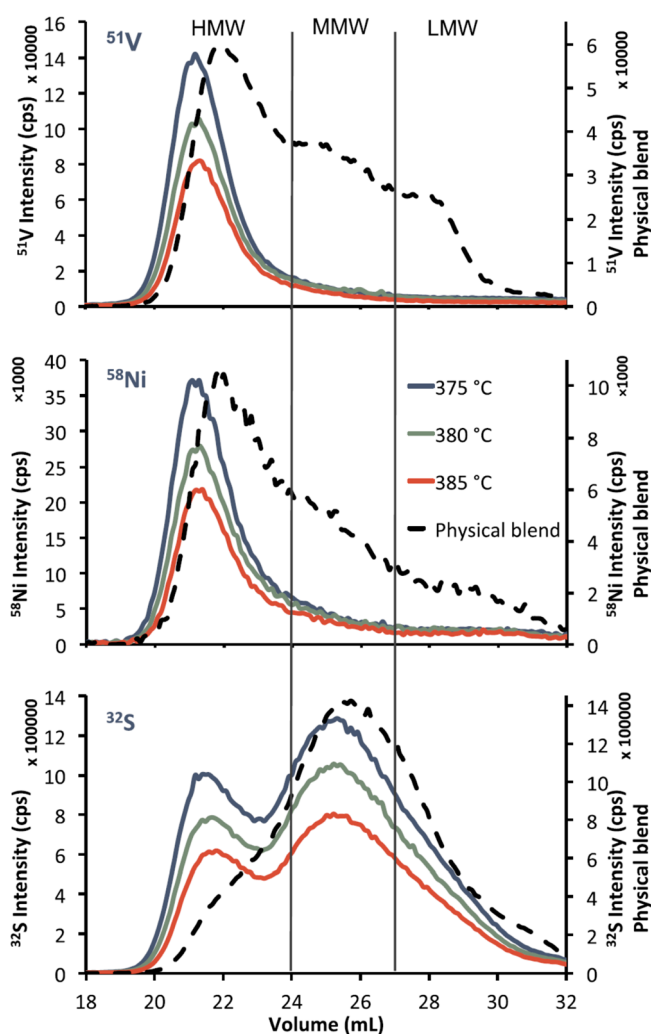

Figure 14. GPC ICP-HR-MS chromatograms of the V, Ni, and S species in the feed (black dashed line) and the product for different temperatures after having been hydrotreated at 375–385 °C and LHSV 0.2 h^{-1}.[78] Reprinted from ref 79. Copyright 2020, with permission from Elsevier.

molecular structures of the most resistant V and Ni in HMW nanoaggregates and to define the stability of their nano-aggregates as a function of temperature.

The distribution for sulfur illustrated in Figure 14 was significantly different, with the remaining sulfur in the remaining asphaltenes detected at significant concentrations in all GPC fractions. These data show that the ease or difficulty of catalytic removal of sulfur is much less correlated with aggregation behavior, indicating that sulfur is not shielded in the same way as vanadium and nickel. A contributing factor may be the wide range of reactivity within each sulfur class. For example, depending on the akyl substitution, the reactivity of the dibenzothiophene homologous series can vary by 1 to 2 orders of magnitude, for the same heteroatomic ring structure.[125]

6. MOLECULAR BASIS FOR DISTRIBUTED NANOAGGREGATE PROPERTIES

The preceding sections of this review discussed the evidence for the distribution of nanoaggregate sizes, based on physical dimensions and molecular weight. Modeling of phase behavior and molecular weight in toluene solutions suggests a range from
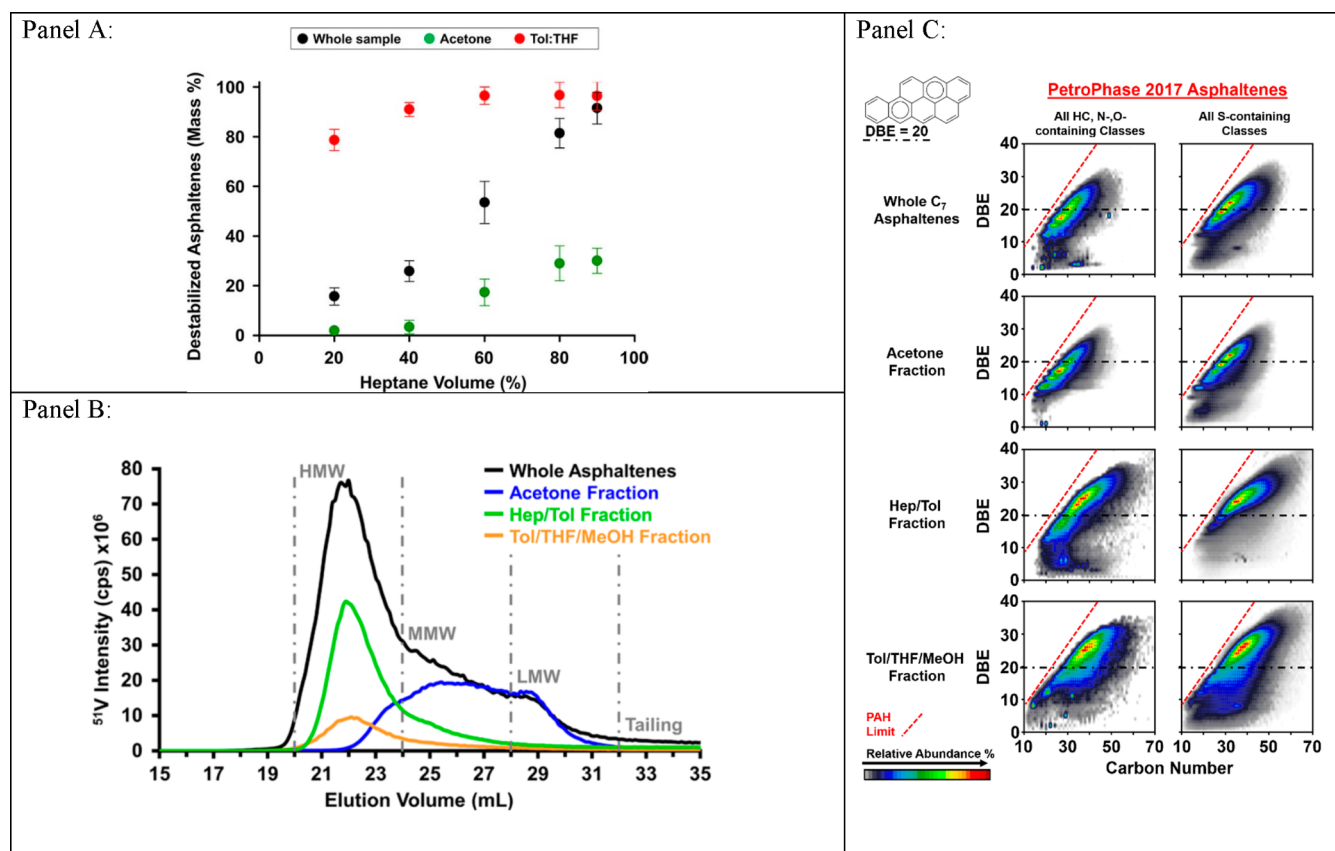
Figure 15. Precipitation (A), GPC elution (B), and molecular composition (C) of extrographic fractions of PetroPhase 2017 asphaltenes.[2,102] Reproduced with permission from refs 2 and 102. Copyright 2018 and 2020, American Chemical Society

asphaltene monomers to 30,000 Da (Figure 10), while nanofiltration suggests a maximum size on the order of 100 nm (Figure 6). GPC analysis gives direct evidence for a distribution of nanoaggregate size (Figure 7), with an approximate upper bound of 30,000 Da based on polystyrene standards.[75] With a monomer molecular weight range from 400 to 1500 Da, the nanoaggregates will range from dimers beginning at 800 Da up to the largest composed of 40−60 molecules. Within this distribution of species, two subfractions stand out as being particularly important:

(a) Large aggregates with high thermal stability, which could serve to prevent reaction of vanadium and other species during catalytic hydroprocessing at 350−400 °C (Figure 14). Given the range of molecular compositions and structures revealed using IRMPD and FT-ICR MS, what are the molecular features that would contribute to high stability of large aggregates? The maximum sizes of the aggregates are important in catalytic hydroprocessing for two reasons. The largest aggregates in the initial feed are most likely to give the most persistent aggregates at reaction conditions, for any conceivable kinetic process of dissociation. Any aggregation of components will dramatically reduce the rate of diffusion into catalyst particles and hinder adsorption to the catalyst surface.

(b) Aggregates with strong affinity for the oil−water interface, which are active in stabilizing water-in-oil emulsions. The fraction of nanoaggregates that adhere strongly to the interface ranges from less than 2% up to 50% depending on the crude oil.[5,97]

6.1. Molecular Features from Extrography and GPC Fractions.
Extrography has shown potential to produce asphaltene fractions with distinctive precipitation (titration with *n*-heptane) and aggregation trends (GPC elution). These data can help to understand the role of molecular properties in the formation of large highly stable aggregates. In the method reported by Chacón-Patiño et al.,[12] asphaltenes are adsorbed on silica gel with a remarkably low mass loading (≤1 wt %) which increases the molecular selectivity for the separation. Subsequently, asphaltenes are extracted through an unconventional solvent series that starts with acetone (with dominant dipole−dipole interactions), then uses toluene/*n*-heptane 1:1 (dispersion forces) and concludes with toluene/tetrahydrofuran/methanol (protic mixture/hydrogen bonding).

Gas-phase fragmentation via IRMPD has shown that the acetone fraction contains abundant island structural motifs, whereas Tol/THF/MeOH is enriched with archipelagos. The acetone fraction from geologically diverse asphaltene samples reveals compounds with higher DBEs and less alkyl substitution compared to the Tol/THF/MeOH fraction. The data of Figure 15 present the precipitation trends accessed by heptane titration of asphaltene solutions in toluene (panel a) and GPC chromatograms (panel b) for whole PetroPhase 2017 asphaltenes and their acetone and Tol/THF fractions. The acetone asphaltenes are less prone to precipitate. For instance, at 60% v/v of heptane, the amount of precipitated material for the whole sample and the Tol/THF fraction is ∼3.0- and ∼5.5-fold higher than the acetone fraction. The longer GPC elution times for the acetone fraction suggest a weaker aggregation tendency, indicating that alkyl-depleted large polynuclear aromatics, with
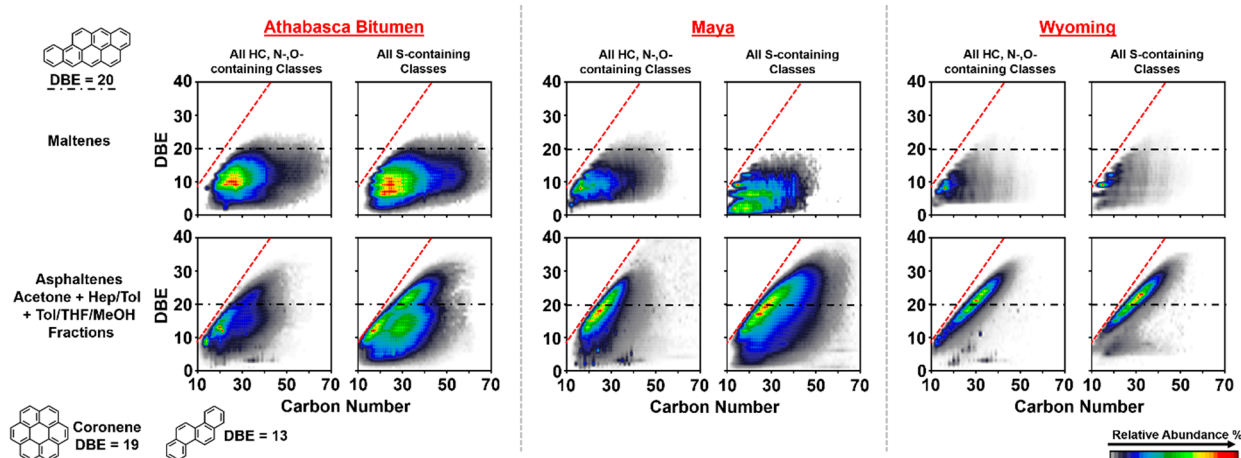
Figure 16. Combined isoabundance color-contoured plots of DBE vs carbon number for HC and N-/O-containing species (plots to the left in each panel) and S-containing compounds (plots to the right) for maltenes (upper row) and all extrography fractions from Athabasca bitumen, Maya, and Wyoming deposit C_7 asphaltenes (lower row). Data derived from (+)APPI 9.4 T FT-ICR-MS characterization. The structures of coronene (a highly pericondensed PAH with DBE = 19) and molecules with DBE = 20 (seven rings) and DBE = 13 (four rings, catacondensed) have been included for reference.

island structural motifs, are not significant drivers of the formation of large nanoaggregates with high stability. Rather, these components have low solubility in *n*-alkanes, giving phase separation along with the much more strongly aggregated fractions.

The data of Figure 15c present the molecular composition of the samples as combined DBE (double bond equivalents = rings plus double bonds) versus carbon number plots for all the species with no sulfur atoms (left plots, i.e., hydrocarbons, HC, N-/O-containing) and all S-containing compounds (right plots, e.g., species with only sulfur, species with both sulfur and oxygen). The black dotted line facilitates sample comparisons based on aromaticity (or hydrogen deficiency); it is placed at DBE 20 since this is the average value for aromatic cores consisting of 6 to 7 fused rings. These results suggest that the acetone fraction contains alkyl-depleted aromatic cores as it reveals abundant molecules clustered close to the polycyclic aromatic hydrocarbon (PAH) limit (red dotted line) with predominant DBE values between 10−30. Therefore, its precipitation/aggregation behaviors suggest that weak π-stacking interactions are likely dominant for the self-assembly of the acetone fraction. Conversely, Hep/Tol and Tol/THF/MeOH fractions reveal longer homologous series (species with equal DBE but varying degrees of carbon number) which translates into a higher content of alkyl moieties and abundant compounds with DBE < 10. The Tol/THF/MeOH fraction is enriched with low-DBE S_xO_y compounds containing both oxygen- and sulfur-containing functionalities, with up to three sulfur and five oxygen atoms in a single molecule.[1] The low aromaticity of those compounds indicates that heteroatom-based interactions rule their aggregation.

Figure 16 presents the combined DBE vs carbon number plots for all compounds with no S atoms (plots to the left in each panel) and all the species with S (plots to the right) for maltenes (alkane soluble) and asphaltenes from Athabasca Bitumen, Maya crude oil, and the Wyoming deposit. The data for asphaltenes are the result of combining the molecular formulas for all the extrography fractions for each of the samples. It is critical to point out that typically, for asphaltenes, at least 90% of the detected ions in +APPI have at least one heteroatom (S, N, O, V). Conversely, maltenes usually present a much higher

relative abundance of "nonpolar" hydrocarbons (HC class, >50%), and the highest heteroatom content is revealed as O_2, S_2, and O_1S_1 classes. Thus, asphaltene species overlapping the compositional range of alkane solubles or maltenes (low carbon number and DBE) have much higher content of heteroatoms (up to seven heteroatoms per molecule, e.g., O_4S_3 class).[36] Their insolubility in alkanes can be explained as molecular insolubility due to high dipolar constants and/or nanoaggregate insolubility as a result of strong aggregation. Figure 16 also demonstrates the ultrahigh diversity of the molecules present in Athabasca bitumen and Maya asphaltenes; the two samples reveal species with low (<20) and high DBE (>20) with little or no alkyl chain content (species clustered on/near the polycyclic aromatic hydrocarbon − PAH limit) and molecules with up to ~40 carbon atoms in alkyl pendant groups (i.e., Maya, S-containing compounds with DBE = 10). In contrast, the Wyoming deposit sample is very "monotonic", with a distribution closer to the PAH boundary with little contribution from diverse heteratomic and archipelago components. Species at the PAH limit, highlighted by a red dotted lined in Figure 16, are hydrogen deficient and have high levels of pericondensation (e.g., coronene, DBE = 19, structure included in Figure 16).[126] It is critical to point out that maltenes reveal no compositions at the PAH limit, whereas asphaltenes feature abundant low-DBE compounds right on that compositional boundary. However, asphaltene species move away from the PAH limit as a function of increasing DBE and carbon number, which suggest the presence of less condensed aromatic structures (catacondensed/archipelago) at higher molecular weight. This implies the existence of a "carbon number/DBE limit" in which molecules cannot support more carbon atoms in the same pericondensed aromatic core (e.g., coronene), and further addition of carbon and hydrogen would likely produce catacondensed moieties (e.g., 4-ring molecule with DBE = 13 shown in Figure 16) and/or archipelago structures.[2,127] Thus, compositional data presented in Figure 16 and structural information published elsewhere[1−4,6,12,128−130] indicate that asphaltenes are an ultra-complex mixture including but not limited to alkyl-depleted PAHs with moderate DBE values and low heteroatom content, alkyl-enriched aromatics with a wide range of aromaticity (DBE = 10−35) and heteroatomic functionalities, and low DBE
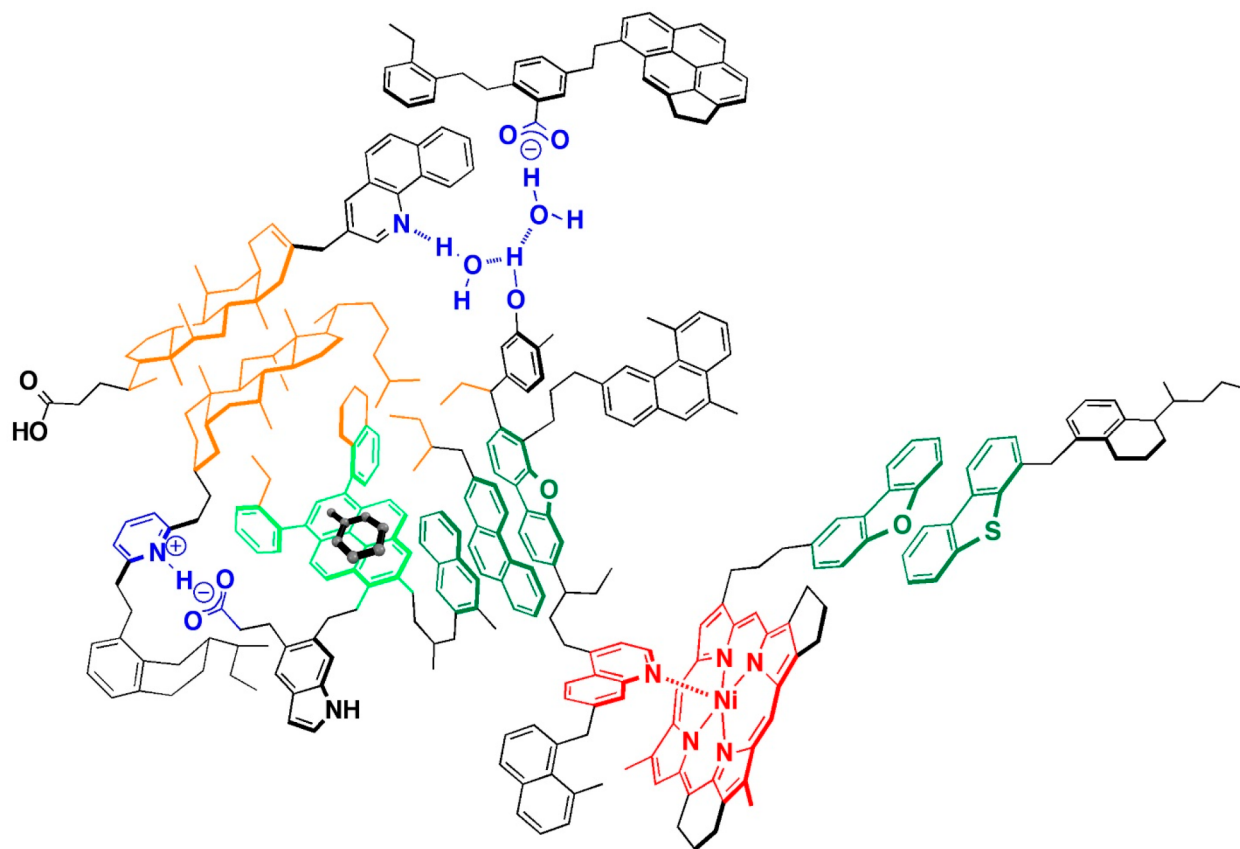
Figure 17. Schematic representation of interactions between archipelago molecules with a variety of functional groups.[131] Reproduced with permission from ref 132. Copyright 2011, American Chemical Society.

Table 6. Parameters to Fit Molecular Weights of Asphaltenes before and after Hydroconversion to Asphaltene Propagation-Termination Model for Aggregation[69]

Sample	Weight fraction of neutrals, w_N	AMW of terminators, M_T	AMW of propagators, M_P	Ratio of terminators to propagators, T/P	Association constant, K
Feed (WR-SR-A3)	0.06	1500	2000	0.06	35000
Remaining after 70% conversion (WR-SR-HC70)	0.22	700	800	0.14	7500
Remaining after 80% conversion (WR-SR-HC80)	0.23	450	650	0.4	7500

Table 7. Intermolecular Interactions Contributing to Formation of Asphaltene Nanoaggregates[132,134]

Intermolecular interaction	Experimental verification
Strong drivers—electron sharing interactions	
(A) Acid—base	Schulze et al.[135]
(B) Free radical pancake bonding[134]	
(C) Charge transfer	Schulze et al.[136]
Medium drivers:	
(A) van der Waals interactions	
(B) Polar groups/electrostatic dipole interactions	Tan et al.[137]
(C) Hydrogen bonding	Tan et al.[138]
Weak to strong depending on the size of the aromatic group and repulsion due to appended groups	
(A) Parallel π−π interactions	Wu et al.,[139] Pisula et al.,[140] Yin et al.[141]
(B) T-shaped π−π interactions	Diner et al.[142]

species with ultrahigh heteroatom contents (polyfunctional compounds, e.g., class O_4S_3). Island and archipelago motifs have been detected for molecules with varying degrees of aromaticity (DBE 15−35) and number of heteroatoms.

6.2. What Molecular Properties Drive Formation of Large Stable Nanoaggregates? The data on the acetone fraction from extrographic separation of asphaltenes indicates clearly that large-ring PAHs with side chains are not strongly

aggregating; therefore, this molecular motif is not dominant in large highly stable nanoaggregates. The extrographic fractions that are enriched in "archipelago" molecular motifs and in heteroatoms, particularly oxygen, give a much higher proportion of HMW aggregates. The critical role of molecules containing multiple groups bridged together is also supported by the process studies discussed in Section 5, which showed that large nanoaggregates were eliminated under processing conditions where carbon−carbon bond breakage was significant. The hydroconversion reactions removed both side chains and pendant aromatic groups, giving lower molecular weight asphaltenes in the product oil with significantly reduced aggregation tendency. These process conditions would also remove oxygen functional groups, including carboxylic acids, sulfones, sulfoxides, and sulfonic acids.

The central importance of the archipelago motif in enabling large stable nanoaggregates is not due to the interactions of the molecular bridges but rather the molecular degrees of freedom to enable multiple groups to interact. Following the principles of supramolecular chemistry, the additive effect of multiple positive interactions between molecules gives a much more stable association of multiple molecules. This range of interactions between archipelago molecules with multiple functional groups is represented conceptually in Figure 17.

Given the known functional groups in petroleum,[6] the list of potential intermolecular forces that could contribute to nanoaggregation has been well defined and is summarized in Table 6.[131,132] Most of these interactions have been verified by detailed study of representative model compounds, as listed in Table 7. Because van der Waals forces are always expected between molecules in close proximity, no specific model compound studies are indicated for this case. When archipelago molecules are abundant in an asphaltene fraction, all these forces can combine to help stabilize an aggregate. This combination of forces can lead to stability at elevated temperature and persistence of nanoaggregates at extremely low concentrations in solvents such as toluene. The lowest concentration studies have been qualitative, based on spectroscopy[38,133] and mass spectrometry.[24]

Asphaltene nanoaggregates are formed from exceedingly complex mixtures of components as supported by the data of Figure 16 and detailed fragmentation studies using IRMPD, chemical-induced dissociation, and thermal reactions, immersed in a multicomponent liquid phase. On the basis of the principles of supramolecular chemistry, the asphaltene components that have complementary structures that enable additive multiple interactions will bind most strongly to each other. For example, a pair of molecular structures that enable combination of ionic interactions by acid−base pairs, $\pi-\pi$ interaction, dipole interaction, and van der Waals interactions of side groups will bind much more strongly than two molecules with only one of these interactions.[131,143] The experimental results of Chacón-Patiño et al.[1] suggest that components with multiple oxygen functional groups will give the strongest aggregation. When the interactions of the molecules are too weak, then the molecules will interact with solvents (or maltenes) as strongly as with each other.

None of the model compound studies listed in Table 6 gave aggregation as stable or as extensive as was observed in actual petroleum asphaltenes. All these studies focused on pure components in solution or binary mixtures of pure components. This observation suggests that the high stability of large nanoaggregates in the asphaltenes may be intrinsic to the complexity of the mixture, enabling a wide range of complementary interactions for a given molecule. For modeling of nanoaggregate formation, the molecular diversity must give rise to a wide range of association constants. For the conceptual nanoaggregate illustrated in Figure 16, an archipelago molecule from solution may interact with a single component on the surface of the aggregate or with more than one component. The latter case would further enhance the stability of the resulting assembly. Modeling of asphaltene aggregation with a range of association constants has been suggested to help to represent this behavior, but the experimental data for validation of such an approach are lacking.[61]

Computational chemistry has significant potential to explore the molecular factors that determine the interactions of asphaltene components in solution and the stability of asphaltene nanoaggregates, but a detailed review and critique of this literature is beyond the scope of this review. Suffice it to note that several limitations must be overcome before such studies can provide conclusive evidence. One limitation is the computational load dealing with sufficiently complex mixtures of molecules with different structural motifs and functional groups, then verifying that equilibrium conditions have been reached.[144] At a more basic level, the ability of the computational methods to accurately represent stability of nanoaggregates in a solvent such as toluene must be calibrated by experimental data and positive and negative controls. In this context, controls verify that the computational methods can reproduce experimental results on actual molecules that undergo nanoaggregation in relevant solvents (positive controls) or that do not undergo detectable nanoaggregation (negative controls). Some promising studies of this type are now beginning to emerge.[145] The molecular dynamics studies tend to attempt to validate results by contrasting the behavior of selected molecules in toluene versus the same species in *n*-heptane. This comparison seeks, incorrectly, to represent the phase separation of asphaltenes as an extension of nanoaggregate formation, without verifying the ability of the computational methods to properly represent nanoaggregates in solution at all.

6.3. What Limits the Maximum Size of Nanoaggregates?
The data from GPC and VPO suggest a maximum molecular weight of ca. 30,000 Da for asphaltene nanoaggregates in good solvents, while nanofiltration suggests a maximum size of ca. 100 nm in stable crude oil. In both cases, the asphaltene monomers range from approximately 400 to 1500 Da. When formation of nanoparticles is observed with pure organic compounds or binary mixtures in solution, three types of behavior are observed:

(a) Indefinite growth, where addition of monomer to ribbon or cylinder structures continues until the monomer is exhausted, giving length scales of micrometers or more.[131]

(b) Limited growth, where addition of monomer to particles or assembly of multimers to form aggregates gives a distribution of sizes up to some limit.[146−149] Methods such as small-angle X-ray and neutron scattering indicate the mean length scale of the aggregates, but as in the case of asphaltenes, the actual distribution is difficult to measure for soft nanoaggregates such as polymers.

(c) Sphere formation, where the geometry of the monomers and their assembly gives a stable micelle or hollow sphere of fixed dimension.[146,148]

The limited growth case is the most relevant to asphaltene nanoparticles which form a distribution of nanoaggregates from

a much more complex mixture of monomers, involving multiple types of intermolecular interactions. Specific geometric interactions of monomers to form hollow spherical assemblies or uniform spheres are unlikely with such complex mixtures. The size of the aggregates is limited by the equilibrium between the monomers in solution and the monomers forming part of a nanoaggregate. Changes in solvent strength, for example, can shift the equilibrium from free monomers in solution toward nanoaggregates and vice versa.[149] An upper bound on nanoaggregates size in petroleum would be set by solubility in the crude oil; too large an aggregate will not be stably dispersed in the oil phase. Although resins can suppress the size of asphaltene aggregates, as illustrated in Figure 9, the removal of weakly aggregating subfractions from the asphaltenes does not give a significant increase in aggregate size based on the data for the THF/TOL/MeOH extrographic subfraction in Figure 15b. The maximum size of nanoaggregates from one fraction was similar to the original asphaltene mixture. Also, when the GPC HMW fractions were extracted and reinjected in xylene, no deaggregation was observed by Putman et al.[150]

The relationship between maximum size of nanaoaggregates in solution and the maximum molecular weight depends on the three-dimensional structure of the nanoaggregates. Two topologies have been proposed most frequently as mean structures: cylindrical one-dimensional stacks with appended side chains[151−153] and mass fractal aggregates.[154,155] Given the diversity of monomer molecules, these topologies are both feasible. Mass fractal aggregates could give distributions of both size and density, but probing of such details is not yet possible experimentally.

6.4. Interfacially Active Nanoaggregates. The surface activity of the nanoaggregates can be interpreted in two ways. They could be flexible structures containing both polar and nonpolar groups and act analogously to a polymer surfactant, or they could be more rigid structures with both polar and nonpolar groups exposed on their surface and act like biwettable particles. The elastic behavior of asphaltene films at the oil−water interface and the slow changes in their properties with time are more consistent with the behavior of some globular proteins, as a potential analogy, than to Pickering emulsions stabilized by rigid solid particles.[94,156]

The topology and size of the asphaltene nanoaggregates that have high affinity for the oil−water interface are likely irrelevant. Single molecules can attach to the interface if they have a sufficiently polar group, such as a carboxylic acid, to provide a hydrophobic end. Molecules with features that we expect in the asphaltene fraction follow this pattern based on model compound studies of substituted perylene bisimides.[157] Alkyl-substituted compounds displayed no interfacial activity, while substitution with alkyl carboxylic acids gave significant adsorption and stacking on the interface. Isolation of the most surface-active fraction of Athabasca asphaltenes showed significant enrichment oxygen, mainly in sulfoxide groups.[158] These groups would be active in hydrogen bonding interactions with water molecules.

A single polar functional group protruding from one of the molecules into solution would likely be sufficient to give interfacial activity for small nanoaggregates composed of a few molecules. The largest nanoaggregates would likely require more than a single polar group to adsorb to the interface. Further study of the surface active asphaltene nanoparticles is required to defined both their size distribution and the concentration of polar functional groups on their surfaces. Like globular proteins

at interfaces, methods to characterize the restructuring and cross-linking of the asphaltene nanoaggregates could give valuable insights, contributing to the design of better demulsification additives.

7. KNOWLEDGE GAPS AND IMPLICATIONS

Although the presence of nanoaggregates in the asphaltene fraction is always a confounding factor in determination of true molecular weight distributions and definition of molecular structure, this review suggests that the details of the aggregate properties and the distribution of those properties are most important for three process applications. First, modeling or controlling the fractionation of the asphaltenes by differential precipitation or by other means requires definition of the distribution of properties, in contrast to predicting the onset of asphaltene deposition or sedimentation where a fraction average will suffice. Second, the catalytic conversion of vacuum residues gives selective conversion of the least nanoaggregated components, while the most strongly aggregated vanadium or nickel is the most resistant to reaction. Third, the adsorption of surface active subfractions of the asphaltenes at oil−water interfaces is important in emulsion stabilization.

In all three cases, direct experimental determination of the distributions or properties at actual processing conditions would be valuable to verify the assumptions of models and to calibrate indirect methods of analysis. The schematic of Figure 10 illustrates a distribution of nanoaggregates consistent with available data, but such a distribution has not been measured directly. Modeling of phase behavior would benefit from validation of inferred distributions of molecular weight and solubility parameter. For catalytic hydrocracking, the GPC profiles are valuable tools to indicate the progress of reactions, but knowledge of the actual persistence of HMW aggregates at temperatures of 350−450 °C and at high dilutions would enable better process and catalyst designs. For emulsion stabilization, information on the distributions of the molecular weight and polar functional groups would define the components of the asphaltene fraction that contribute most strongly to the formation of stable interfacial films. For instance, recent studies demonstrate that interfacial material (IM) extracted from asphaltenes contains abundant O_xS_y species with up to seven heteroatoms per molecule. These molecules feature low aromaticity and preferentially ionize via protonation, which agree with their capability to hydrogen bond in solution.[36] Furthermore, their GPC elution profiles point to the existence of bigger nanoaggregates that elute earlier than the large aggregates of whole/unfractionated asphaltene samples.

The synthesis of model compounds for asphaltenes, as summarized in Table 7, has given insights into the interactions of different functional groups in solution and the behavior of individual molecules at oil−water interfaces.[157] These bottom-up approaches have not given stable HMW aggregates or rigid interfacial films because the model mixtures do not replicate key nanoaggregate properties. Functionalized gold nanoparticles have been suggested as a model for interfacial behavior of asphaltenes.[159] Depending on the surface groups, these particles mimic some thermodynamic and interfacial tension properties of asphaltenes, but they are unlikely to show the film behaviors that are so important in emulsion stabilization. Highly branched or cross-linked polymers can give nanoparticles,[160,161] but such models cannot dissociate with temperature or concentration like the asphaltenes nor are they likely to restructure at interfaces. Soft nanoparticles formed by the self-assembly of small

molecules may have potential as models for asphaltene nanoaggregates. However, only a few studies have reported appropriate molecular weights and length scales, and these examples are limited to aqueous solutions.[146−148]

A more promising approach is the fractionation of asphaltenes to obtain mixtures with either a very narrow range of properties or to combine fractions to create unusual distributions of properties to investigate specific hypotheses. For example, samples that are highly enriched in island-type structures with weak aggregation can be prepared from sources such as the Wyoming deposit.[2] Crude oils may also exist with such extreme properties, and processed samples such as asphaltenes after hydroconversion of vacuum residue are a likely source.[69] At the opposite extreme, heavy oils and bitumens are enriched in archipelago fractions that give stable aggregation.[36] Scale-up of the extrographic technique or use of preparative GPC are promising methods for preparing such asphaltene subfractions with narrow ranges of properties. In contrast to "whole" asphaltenes recovered from phase separations, which contain an incredibly diverse range of molecular and nanoaggregate types, studies of such defined subfractions and their mixtures have great promise to define the role of molecular components and to support robust quantitative models for asphaltene behavior.

■ CONCLUSIONS

The chemical and aggregation behaviors of fractionated samples demonstrate that association of asphaltene molecules to form nanoaggregates in solution is mainly driven by polar interactions of archipelago species. The molecular weight of nanoaggregates may range as high as 40,000 Da, with a range of sizes below 100 nm. The distribution of nanoaggregates in solution has little impact on the onset of phase separation but plays a role in determining the yield of fractions from partial removal of the asphaltene fraction. The distribution of size or properties of nanoaggregates has little impact on density or on viscosity behavior in the Newtonian regime. The impact of nanoaggregate distributions is most significant in properties of films at oil/water interfaces in stabilization of surface films and in catalytic hydrogenation of vanadium and nickel compounds.

■ AUTHOR INFORMATION

Corresponding Author

   Murray R. Gray − *Department of Chemical and Materials Engineering, University of Alberta, Edmonton, AB, Canada T6G 1H9;* ● orcid.org/0000-0003-2431-7312;
   Email: murray.gray@ualberta.ca

Authors

   Harvey W. Yarranton − *Department of Chemical and Petroleum Engineering, University of Calgary, Calgary, AB, Canada T2N 1N4;* ● orcid.org/0000-0002-7726-5061

   Martha L. Chacón-Patiño − *Ion Cyclotron Resonance Program, National High Magnetic Field Laboratory, Florida State University, Tallahassee, Florida 32310, United States; International Joint Laboratory iC2MC: Complex Matrices Molecular Characterization, Total Research & Technology, Gonfreville 76700 Harfleur, France;* ● orcid.org/0000-0002-7273-5343

   Ryan P. Rodgers − *Ion Cyclotron Resonance Program, National High Magnetic Field Laboratory, Florida State University, Tallahassee, Florida 32310, United States; International Joint Laboratory iC2MC: Complex Matrices Molecular Characterization, Total Research & Technology, Gonfreville*

76700 Harfleur, France; ● orcid.org/0000-0003-1302-2850

   Brice Bouyssiere − *International Joint Laboratory iC2MC: Complex Matrices Molecular Characterization, Total Research & Technology, Gonfreville 76700 Harfleur, France; E2S UPPA, CNRS, IPREM, Institut des Sciences Analytiques et de Physico-chimie pour l'Environnement et les Materiaux, Universite de Pau et des Pays de l'Adour, 64053 Pau, France;* ● orcid.org/0000-0001-5878-6067

   Pierre Giusti − *International Joint Laboratory iC2MC: Complex Matrices Molecular Characterization, Total Research & Technology, Gonfreville 76700 Harfleur, France; E2S UPPA, CNRS, IPREM, Institut des Sciences Analytiques et de Physico-chimie pour l'Environnement et les Materiaux, Universite de Pau et des Pays de l'Adour, 64053 Pau, France; TOTAL Refining and Chemicals, Total Research and Technology Gonfreville (TRTG), 76700 Harfleur, France;* ● orcid.org/0000-0002-9569-3158

Complete contact information is available at:
https://pubs.acs.org/10.1021/acs.energyfuels.1c01837

Notes

The authors declare no competing financial interest.

Biographies

Murray R. Gray is Professor Emeritus of chemical engineering at the University of Alberta and Senior Technical Advisor at Alberta Innovates. He has over 30 years of research experience in upgrading of heavy oil and oil sands bitumen. Gray obtained his Ph.D. in chemical engineering from the California Institute of Technology in 1984. He also holds a M.Eng. from the University of Calgary (1980) and a B.Sc. in chemical engineering from the University of Toronto (1978).

Harvey W. Yarranton is a Professor of chemical and petroleum engineering at the University of Calgary. He received his B.Sc. (1985) and Ph.D. (1997) degrees in chemical engineering from the University of Alberta. Between degrees, he worked for Dome Petroleum Ltd. and Amoco Canada Ltd. in reservoir, production, and operations engineering. His research interests include the phase behavior and properties of heavy oils and solvents, the fundamentals and treatment of water-in-oil emulsions, and oil sands extraction and froth treatment.

Martha L. Chacón-Patiño is a faculty member of the National High Magnetic Field Laboratory in Tallahassee, Florida. Chacón-Patiño obtained her Ph.D. in chemistry from the Industrial University of Santander in Bucaramanga, Colombia (2016). She is an expert in the characterization of complex organic mixtures by separations and ultrahigh-resolution mass spectrometry (e.g., asphaltenes, biofuels, and emerging contaminants).

Ryan P. Rodgers received a B.S. (chemistry) from the University of Florida and a Ph.D. (analytical chemistry) from Florida State University. After a postdoctoral appointment at Oak Ridge National Laboratory, he joined the Ion Cyclotron Resonance Program at the National High Magnetic Field Laboratory (Florida State University). He is currently a Research Faculty III, the Director of the Future Fuels Institute, an FSU Distinguished University Scholar, and a past Associate Editor of *Energy and Fuels*.

Brice Bouyssiere is Professor of analytical chemistry at the University of Pau and cofounder and coresponsible of the International Lab on Complex Matrices Molecular Characterization (iC2MC lab). After

Chemical and Process Engineering School (ENSGTI) and a Ph.D. dealing with speciation of mercury and arsenic in gas condensates at the University of Pau, he did a postdoctoral stay at GKSS Geesthacht, Germany. His principal research interest is metals speciation in complex matrices.

Pierre Giusti obtained his Ph.D. in analytical chemistry from the University of Pau and Pays de l'Adour in 2006. He is currently the manager of the Molecular Separation and Identification Service in R&D department of TotalEnergies Refining & Chemicals. As cofounder of the iC2MC laboratory, he also obtained the position of CNRS Research Director in January 2021. His research interests are the elemental and molecular analyses of complex matrices in the field of energy.

◼ ABBREVIATIONS

FT-ICR MS = Fourier-transform ion-cyclotron resonance mass spectrometry
GPC = gel permeation chromatography
HMW = high molecular weight fraction
ICP HR = MS ion-coupled plasma high-resolution mass spectrometry
IRMPD = infrared multiphoton dissociation
LMW = low molecular weight fraction
MMW = medium molecular weight fraction
SAXS = small-angle X-ray scattering
VPO = vapor pressure osmometry

◼ REFERENCES

(1) Chacón-Patiño, M. L.; Smith, D. F.; Hendrickson, C. L.; Marshall, A. G.; Rodgers, R. P. Advances in Asphaltene Petroleomics. Part 4. Compositional Trends of Solubility Subfractions Reveal that Polyfunctional Oxygen-Containing Compounds Drive Asphaltene Chemistry. *Energy Fuels* **2020**, *34*, 3013−3030.

(2) Chacón-Patiño, M. L.; Rowland, S. M.; Rodgers, R. P. Advances in Asphaltene Petroleomics. Part 3. Dominance of Island or Archipelago Structural Motif Is Sample Dependent. *Energy Fuels* **2018**, *32*, 9106−9120.

(3) Rogel, E.; Witt, M. Asphaltene Characterization during Hydroprocessing by Ultrahigh-Resolution Fourier Transform Ion Cyclotron Resonance Mass Spectrometry. *Energy Fuels* **2017**, *31*, 3409−3416.

(4) Chacón-Patiño, M. L.; Rowland, S. M.; Rodgers, R. P. Advances in asphaltene petroleomics. Part 1: Asphaltenes are composed of abundant island and archipelago structural motifs. *Energy Fuels* **2017**, *31*, 13509−13518.

(5) Yang, X. L.; Hamza, H.; Czarnecki, J. Investigation of subfractions of Athabasca asphaltenes and their role in emulsion stability. *Energy Fuels* **2004**, *18*, 770−777.

(6) Strausz, O. P.; Lown, E. M. *The Chemistry of Alberta Oil Sands, Bitumens, and Heavy Oils*; Alberta Energy Research Institute: Calgary, AB, 2003; p 695.

(7) Juyal, P.; McKenna, A. M.; Fan, T. G.; Cao, T.; Rueda-Velasquez, R. I.; Fitzsimmons, J. E.; Yen, A.; Rodgers, R. P.; Wang, J. X.; Buckley, J. S.; et al. Joint Industrial Case Study for Asphaltene Deposition. *Energy Fuels* **2013**, *27* (4), 1899−1908.

(8) Schuler, B.; Fatayer, S.; Meyer, G.; Rogel, E.; Moir, M.; Zhang, Y.; Harper, M. R.; Pomerantz, A. E.; Bake, K. D.; Witt, M.; et al. Heavy Oil Based Mixtures of Different Origins and Treatments Studied by Atomic Force Microscopy. *Energy Fuels* **2017**, *31*, 6856−6861.

(9) Zhang, Y.; Schulz, F.; Rytting, B.; Walters, C.; Kaiser, K.; Metz, J.; Harper, M.; Merchant, S.; Mennito, A.; Qian, K.; et al. Elucidating the Geometric Substitution of Petroporphyrins by Spectroscopic Analysis and AFM Molecular Imaging. *Energy Fuels* **2019**, *33*, 6088−6097.

(10) Schuler, B.; Meyer, G.; Pena, D.; Mullins, O. C.; Gross, L. Unraveling the Molecular Structures of Asphaltenes by Atomic Force Microscopy. *J. Am. Chem. Soc.* **2015**, *137* (31), 9870−9876.

(11) Chacón-Patiño, M. L.; Rowland, S. M.; Rodgers, R. P. *The Compositional and Structural Continuum of Petroleum from Light Distillates to Asphaltenes: The Boduszynski Continuum Theory As Revealedby FT-ICR Mass Spectrometry*; American Chemical Society: Washington, DC, 2018; Vol. *1282*, pp 113−171.

(12) Chacón-Patiño, M. L.; Rowland, S. M.; Rodgers, R. P. Advances in Asphaltene Petroleomics. Part 2: Selective Separation Method That Reveals Fractions Enriched in Island and Archipelago Structural Motifs by Mass Spectrometry. *Energy Fuels* **2018**, *32*, 314−328.

(13) Rodgers, R. P.; Mapolelo, M. M.; Robbins, W. K.; Chacón-Patiño, M. L.; Putman, J. C.; Niles, S. F.; Rowland, S. M.; Marshall, A. G. Combating selective ionization in the high resolution mass spectral characterization of complex mixtures. *Faraday Discuss.* **2019**, *218*, 29−51.

(14) Giraldo-Dávila, D.; Chacón-Patiño, M. L.; McKenna, A. M.; Blanco-Tirado, C.; Combariza, M. Y. Correlations between Molecular Composition and Adsorption, Aggregation, and Emulsifying Behaviors of PetroPhase 2017 Asphaltenes and Their Thin-Layer Chromatography Fractions. *Energy Fuels* **2018**, *32*, 2769−2780.

(15) McKenna, A. M.; Chacón-Patiño, M. L.; Weisbrod, C. R.; Blakney, G. T.; Rodgers, R. P. Molecular-Level Characterization of Asphaltenes Isolated from Distillation Cuts. *Energy Fuels* **2019**, *33*, 2018−2029.

(16) Chacón-Patiño, M. L.; Blanco-Tirado, C.; Orrego-Ruiz, J. A.; Gómez-Escudero, A.; Combariza, M. Y. High Resolution Mass Spectrometric View of Asphaltene-SiO2 Interactions. *Energy Fuels* **2015**, *29*, 1323−1331.

(17) Rogel, E.; Witt, M.; Moir, M. E. Effects of Aging on Asphaltene Deposit Composition Using Ultrahigh-Resolution Magnetic Resonance Mass Spectrometry. *Energy Fuels* **2019**, *33*, 9596−9603.

(18) Ballard, D. A.; Chacón-Patiño, M. L.; Qiao, P.; Roberts, K. J.; Rae, R.; Dowding, P. J.; Xu, Z.; Harbottle, D. Molecular Characterization of Strongly and Weakly Interfacially Active Asphaltenes by High-Resolution Mass Spectrometry. *Energy Fuels* **2020**, *34*, 13966−1397.

(19) Nellensteyn, F. J. *Bereiding en constitutie van asphalt (Manufacture and constitution of asphaltic bitumen)*. Dissertatie Technische Hoogeschool, Delft, Netherlands, 1923.

(20) Pfeiffer, J. P.; Saal, R. N. J. Asphaltic bitumen as a colloid system. *J. Phys. Chem.* **1940**, *44*, 139−145.

(21) Brown, T. H.; Gutowsky, H. S.; Van Holde, K. E. Electron Spin Resonance and Colloidal Properties of Crude Oil. *J. Chem. Eng. Data* **1960**, *5*, 181−182.

(22) Zhao, B.; Shaw, J. M. Composition and size distribution of coherent nanostructures in Athabasca bitumen and Maya crude oil. *Energy Fuels* **2007**, *21* (5), 2795−2804.

(23) Dechaine, G. P.; Gray, M. R. Membrane diffusion measurements do not detect exchange between asphaltene aggregates and solution phase. *Energy Fuels* **2011**, *25*, 509−523.

(24) McKenna, A. M.; Donald, L. J.; Fitzsimmons, J. E.; Juyal, P.; Spicer, V.; Standing, K. G.; Marshall, A. G.; Rodgers, R. P. Heavy petroleum composition. 3. Asphaltene aggregation. *Energy Fuels* **2013**, *27* (3), 1246−1256.

(25) Natarajan, A.; Xie, J.; Wang, S.; Masliyah, J. H.; Zeng, H.; Xu, Z. Understanding molecular interactions of asphaltenes in organic solvents using a surface force apparatus. *J. Phys. Chem. C* **2011**, *115* (32), 16043−16051.

(26) Yarranton, H. W.; Ortiz, D. P.; Barrera, D. M.; Baydak, E. N.; Barre, L.; Frot, D.; Eyssautier, J.; Zeng, H.; Xu, Z.; Dechaine, G.; et al. On the Size Distribution of Self-Associated Asphaltenes. *Energy Fuels* **2013**, *27* (9), 5083−5106.

(27) Maqbool, T.; Raha, S.; Hoepfner, M. P.; Fogler, H. S. Modeling the Aggregation of Asphaltene Nanoaggregates in Crude Oil-Precipitant Systems. *Energy Fuels* **2011**, *25* (4), 1585−1596.

(28) Duran, J. A.; Schoeggl, F. F.; Yarranton, H. W.; Favero, C. V. B.; Fogler, H. S. Effect of Air on the Kinetics of Asphaltene Precipitation from Diluted Crude Oils. *Energy Fuels* **2020**, *34* (2), 1408−1421.

(29) Duran, J. A.; Schoeggl, F. F.; Yarranton, H. W. Kinetics of asphaltene precipitation/aggregation from diluted crude oil. *Fuel* **2019**, *255*, 115859.

(30) Yang, Y.; Chaisoontornyotin, W.; Hoepfner, M. P. Structure of asphaltenes during precipitation investigated by ultra-small-angle x-ray scattering. *Langmuir* **2018**, *34*, 10371−10380.

(31) AlHammadi, A. A.; Chen, Y.; Yen, A.; Wang, J.; Creek, J. L.; Vargas, F. M.; Chapman, W. G. Effect of the gas composition and gas/oil ratio on asphaltene deposition. *Energy Fuels* **2017**, *31*, 3610−3619.

(32) Zou, X. Y.; Zhang, X. H.; Shaw, J. M. Phase behavior of Athabasca vacuum bottoms plus *n*-alkane mixtures. *SPE Prod. Oper.* **2007**, *22* (2), 265−272.

(33) Johnston, K. A.; Schoeggl, F. F.; Satyro, M. A.; Taylor, S. D.; Yarranton, H. W. Phase behavior of bitumen and n-pentane. *Fluid Phase Equilib.* **2017**, *442*, 1−19.

(34) Ramos-Pallares, F.; Yarranton, H. W. Extending the Modified Regular Solution Model To Predict Component Partitioning to the Asphaltene-Rich Phase. *Energy Fuels* **2020**, *34*, 5213−5230.

(35) Yarranton, H. W.; Schoeggl, F. S.; George, S.; Taylor, S. D. Asphaltene-Rich Phase Compositions and Sediment Volumes from Drying Experiments. *Energy Fuels* **2011**, *25* (8), 3624−3633.

(36) Chacón-Patiño, M. L.; Gray, M. R.; Niles, S. F.; Glattke, T.; Moulian, R.; Putman, J.; Smith, D. F.; McKenna, A. M.; Weisbord, C. W.; Giusti, P. Lessons Learned from a Long-Decade Assessment of Asphaltenes By Ultra-High-Resolution Mass Spectrometry and Implications for Complex Mixture Analysis. *Energy Fuels* **2021**.

(37) Yarranton, H. W.; Alboudwarej, H.; Jakher, R. Investigation of asphaltene association with vapor pressure osmometry and interfacial tension measurements. *Ind. Eng. Chem. Res.* **2000**, *39*, 2916−2924.

(38) Evdokimov, I. N.; Fesan, A. A. Multi-step formation of asphaltene colloids in dilute solutions. *Colloids Surf., A* **2016**, *492*, 170−180.

(39) Zhang, H. T.; Li, R.; Yang, Z.; Yin, C.-X.; Gray, M. R.; Bohne, C. Evaluating steady-state and time-resolved fluorescence as a tool to study the behavior of asphaltene in toluene. *Photochemical & Photobiological Sciences* **2014**, *13*, 917−928.

(40) Hall, G.; Perron, S. P., Size Characterization of Petroleum Asphaltenes and Maltenes. In *Chemistry of Asphaltenes*; Bunger, J. W., Li, N. C., Eds.; American Chemical Society: Washington DC, 1982; Vol. *195*, pp 137−153.

(41) Gray, M. R. *Upgrading Oilsands Bitumen and Heavy Oil*; University of Alberta Press: Edmonton, AB, 2015; p 499.

(42) Tavakkoli, M.; Panuganti, S. R.; Taghikhani, V.; Pishvaie, M. R.; Chapman, W. G. Understanding the polydisperse behavior of asphaltenes during precipitation. *Fuel* **2014**, *117*, 206−217.

(43) Canas-Marín, W. A.; Gonzalez, D. L.; Hoyos, B. A. A theoretically modified PC-SAFT equation of state for predicting asphaltene onset pressures at low temperatures. *Fluid Phase Equilib.* **2019**, *495*, 1−11.

(44) Li, Z.; Firoozabadi, A. Cubic-Plus-Association Equation of State for Asphaltene Precipitation in Live Oils. *Energy Fuels* **2010**, *24*, 2956−2963.

(45) Arya, A.; Liang, X.; von Solms, N.; Kontogeorgis, G. M. Modeling of Asphaltene Precipitation from Crude Oil with the Cubic Plus Association Equation of State. *Energy Fuels* **2017**, *31*, 2063−2075.

(46) Barrera, D. M.; Ortiz, D. P.; Yarranton, H. W. Molecular Weight and Density Distributions of Asphaltenes from Crude Oils. *Energy Fuels* **2013**, *27*, 2474−2487.

(47) Bazyleva, A.; Fulem, M.; Becerra, M.; Zhao, B.; Shaw, J. M. Phase Behavior of Athabasca Bitumen. *J. Chem. Eng. Data* **2011**, *56* (7), 3242−3253.

(48) Zhang, Y.; Takanohashi, T.; Sato, S.; Saito, I.; Tanaka, R. Observation of Glass Transition in Asphaltenes. *Energy Fuels* **2004**, *18*, 283−284.

(49) Gray, M. R.; Assenheimer, G.; Boddez, L.; McCaffrey, W. C. Melting and fluid behavior of asphaltene films at 200−500 °C. *Energy Fuels* **2004**, *18*, 1419−1423.

(50) Nciri, N.; Song, S.; Kim, N.; Cho, N. Chemical Characterization of Gilsonite Bitumen. *J. Pet. Environ. Biotechnol.* **2014**, *05*, 1000193.

(51) Fadaei, H.; Shaw, J. M.; Sinton, D. Bitumen-Toluene Mutual Diffusion Coefficients Using Microfluidics. *Energy Fuels* **2013**, *27*, 2042−2048.

(52) Zielinski, J. M.; Duda, J. L. Predicting Poly mer/Solven t Diffusion Coefficients Using Free-Volume Theory. *AIChE J.* **1992**, *38*, 405−415.

(53) Pal, R. Modeling and Scaling of the Viscosity of Suspensions of Asphaltene Nanoaggregates. *Energies* **2017**, *10*, 767.

(54) Eyssautier, J.; Henaut, I.; Levitz, P.; Espinat, D.; Barre, L. Organization of Asphaltenes in a Vacuum Residue: A Small-Angle X-ray Scattering (SAXS) Viscosity Approach at High Temperatures. *Energy Fuels* **2012**, *26*, 2696−2704.

(55) Abivin, P.; Taylor, S. D.; Freed, F. Thermal Behavior and Viscoelasticity of Heavy Oils. *Energy Fuels* **2012**, *26*, 3448−3461.

(56) Gawrys, K. L.; Blankenship, G. A.; Kilpatrick, P. K. On the distribution of chemical properties and aggregation of solubility fractions in asphaltenes. *Energy Fuels* **2006**, *20* (2), 705−714.

(57) Rogel, E.; Roye, M.; Vien, J.; Miao, T. Characterization of Asphaltene Fractions: Distribution, Chemical Characteristics, and Solubility Behavior. *Energy Fuels* **2015**, *29* (4), 2143−2152.

(58) McKay Rytting, B.; Singh, I. D.; Kilpatrick, P. K.; Harper, M. R.; Mennito, A. S.; Zhang, Y. Ultrahigh-Purity Vanadyl Petroporphyrins. *Energy Fuels* **2018**, *32*, 5711−5724.

(59) Kharrat, A. Characterization of Canadian Heavy Oils Using Sequential Extraction Approach. *Energy Fuels* **2009**, *23*, 828−834.

(60) Wang, S.; Yang, C.; Xu, C.; Zhao, S.; Shi, Q. Separation and characterization of petroleum asphaltene fractions by ESI FT-ICR MS and UV-vis spectrometer. *Sci. China: Chem.* **2013**, *56*, 856−862.

(61) Gray, M. R.; Yarranton, H. W. Quantitative Modeling of Formation of Asphaltene Nanoaggregates. *Energy Fuels* **2019**, *33* (9), 8566−8575.

(62) Gascon, G.; Vargas, V.; Feo, L.; Castellano, O.; Castillo, J.; Giusti, P.; Acavedo, S.; Lienemann, C. P.; Bouyssiere, B. Size Distributions of Sulfur, Vanadium, and Nickel Compounds in Crude Oils, Residues, and Their Saturate, Aromatic, Resin, and Asphaltene Fractions Determined by Gel Permeation Chromatography Inductively Coupled Plasma High-Resolution Mass Spectrometry. *Energy Fuels* **2017**, *31* (8), 7783−7788.

(63) Wu, Q.; Pomerantz, A. E.; Mullins, O. C.; Zare, R. N. Laser-Based Mass Spectrometric Determination of Aggregation Numbers for Petroleum- and Coal-Derived Asphaltenes. *Energy Fuels* **2014**, *28* (1), 475−482.

(64) Marques, J.; Merdrignac, I.; Baudot, A.; Barre, L.; Guillaume, D.; Espinat, D.; Brunet, S. Asphaltenes size polydispersity reduction by nano- and ultrafiltration separation methods - Comparison with the flocculation method. *Oil Gas Sci. Technol.* **2008**, *63* (1), 139−149.

(65) Marques, J.; Guillaume, D.; Merdrignac, I.; Espinat, D.; Barre, L.; Brunet, S. Asphaltene Cross-flow Membrane Ultrafiltration on a Preparative Scale and Feedstock Reconstitution Method. *Oil Gas Sci. Technol.* **2009**, *64* (6), 795−806.

(66) Ray, B. R.; Witherspoon, P. A.; Grim, R. E. A Study of the Colloidal Characteristics of Petroleum using the Ultracentrifuge. *J. Phys. Chem.* **1957**, *61*, 1296−1302.

(67) Barre, L.; Simon, S.; Palermo, T. Solution properties of asphaltenes. *Langmuir* **2008**, *24* (8), 3709−3717.

(68) Mostowfi, F.; Indo, K.; Mullins, O. C.; McFarlane, R. Asphaltene nanoaggregates studied by centrifugation. *Energy Fuels* **2009**, *23*, 1194−1200.

(69) Powers, D. P.; Sadeghi, H.; Yarranton, H. W.; van den Berg, F. G. A. Regular solution based approach to modeling asphaltene precipitation from native and reacted oils: Part 1, molecular weight, density, and solubility parameter distributions of asphaltenes. *Fuel* **2016**, *178*, 218−233.

(70) Agrawala, M.; Yarranton, H. W. An asphaltene association model analogous to linear polymerization. *Ind. Eng. Chem. Res.* **2001**, *40*, 4664−4672.

(71) Zuo, J. Y.; Mullins, O. C.; Freed, D.; Elshahawi, H.; Dong, C. L.; Seifert, D. J. Advances in the Flory-Huggins-Zuo Equation of State for Asphaltene Gradients and Formation Evaluation. *Energy Fuels* **2013**, *27* (4), 1722−1735.

(72) Zuo, J. L. Y.; Mullins, O. C.; Freed, D.; Zhang, D.; Dong, C. L.; Zeng, H. A. Analysis of Downhole Asphaltene Gradients in Oil

Reservoirs with a New Bimodal Asphaltene Distribution Function. *J. Chem. Eng. Data* **2011**, *56* (4), 1047−1058.

(73) Rogel, E.; Ovalles, C.; Bake, K. D.; Zuo, J. Y.; Dumont, H.; Pomerantz, A. E.; Mullins, O. C. Asphaltene Densities and Solubility Parameter Distributions: Impact on Asphaltene Gradients. *Energy Fuels* **2016**, *30*, 9132−9140.

(74) Panuganti, S. R.; Vargas, F. M.; Chapman, W. G. Modeling Reservoir Connectivity and Tar Mat Using Gravity-Induced Asphaltene Compositional Grading. *Energy Fuels* **2012**, *26* (5), 2548−2557.

(75) Merdrignac, I.; Quoineaud, A. A.; Gauthier, T. Evolution of asphaltene structure during hydroconversion conditions. *Energy Fuels* **2006**, *20* (5), 2028−2036.

(76) Gutierrez Sama, S.; Desprez, A.; Krier, G.; Lienemann, C.-P.; Barbier, J.; Lobinski, R.; Barrere-Mangote, C.; Giusti, P.; Bouyssiere, B. Study of the Aggregation of Metal Complexes with Asphaltenes Using Gel Permeation Chromatography Inductively Coupled Plasma High-Resolution Mass Spectrometry. *Energy Fuels* **2016**, *30* (9), 6907−6912.

(77) Pohl, P.; Dural, J.; Vorapalawut, N.; Merdrignac, I.; Lienemann, C. P.; Carrier, H.; Grassl, B.; Bouyssiere, B.; Lobinski, R. Multielement molecular size fractionation in crude oil and oil residue by size exclusion microchromatography with high resolution inductively coupled plasma mass spectrometric detection (HR ICP MS). *J. Anal. At. Spectrom.* **2010**, *25* (12), 1974−1977.

(78) Garcia-Montoto, V.; Verdier, S.; Maroun, Z.; Egeberg, R.; Tiedje, J. L.; Sandersen, S.; Zeuthen, P.; Bouyssiere, B. Understanding the removal of V, Ni and S in crude oil atmospheric residue hydro-demetallization and hydrodesulfurization. *Fuel Process. Technol.* **2020**, *201*, 106341.

(79) Barbier, J.; Gaulier, F.; Guichard, B.; Levitz, P.; Espinat, D. Asphaltenes Transport into Hydroconversion Catalysts at High Temperature: Role of the Alumina Nanoporous Texture. *Energy Fuels* **2017**, *31* (7), 7426−7437.

(80) Baltus, R. E.; Anderson, J. L. Hindered diffusion of asphaltenes through microporous membranes. *Chem. Eng. Sci.* **1983**, *38* (12), 1959−1969.

(81) Akbarzadeh, K.; Alboudwarej, H.; Svrcek, W. Y.; Yarranton, H. W. A generalized regular solution model for asphaltene precipitation from *n*-alkane diluted heavy oils and bitumens. *Fluid Phase Equilib.* **2005**, *232*, 159−170.

(82) Czarnecki, J.; Moran, K. On the stabilization mechanism of water-in-oil emulsions in petroleum systems. *Energy Fuels* **2005**, *19*, 2074−2079.

(83) Czarnecki, J.; Tchoukov, P.; Dabros, T. Possible Role of Asphaltenes in the Stabilization of Water-in-Crude Oil Emulsions. *Energy Fuels* **2012**, *26* (9), 5782−5786.

(84) Tchoukov, P.; Yang, F.; Xu, Z.; Dabros, T.; Czarnecki, J.; Sjöblom, J. Role of asphaltenes in stabilizing thin liquid emulsion films. *Langmuir* **2014**, *30*, 3024−3033.

(85) Sztukowski, D. M.; Jafari, M.; Alboudwarej, H.; Yarranton, H. W. Asphaltene self-association and water-in-hydrocarbon emulsions. *J. Colloid Interface Sci.* **2003**, *265* (1), 179−186.

(86) Rane, J. P.; Harbottle, D.; Pauchard, V.; Couzis, A.; Banerjee, S. Adsorption Kinetics of Asphaltenes at the Oil-Water Interface and Nanoaggregation in the Bulk. *Langmuir* **2012**, *28*, 9986−9995.

(87) Jeribi, M.; Almir-Assad, B.; Langevin, D.; Henaut, I.; Argillier, J. F. Adsorption Kinetics of Asphaltenes at Liquid Interfaces. *J. Colloid Interface Sci.* **2002**, *256*, 268−272.

(88) Yarranton, H. W.; Sztukowski, D. M.; Urrutia, P. Effect of interfacial rheology on model emulsion coalescence (Part I). *J. Colloid Interface Sci.* **2007**, *310*, 246−252.

(89) Mohammed, R. A.; Bailey, A. I.; Luckham, P. F.; Taylor, S. E. Dewatering of crude oil emulsions 1. Rheological behaviour of the crude oil-water interface. *Colloids Surf., A* **1993**, *80*, 223−235.

(90) Spiecker, P. M.; Kilpatrick, P. K. Interfacial Rheology of Petroleum Asphaltenes at the Oil-Water Interface. *Langmuir* **2004**, *20*, 4022−4032.

(91) Freer, E. M.; Radke, C. J. Relaxation of Asphaltenes at the Toluene/Water Interface: Diffusion Exchange and Surface Rearrangement. *J. Adhes.* **2004**, *80*, 481.

(92) Yeung, T.; Dabros, T.; Czarnecki, J.; Masliyah, J. H. On the interfacial properties of micrometre-sized water droplets in crude oil. *Proc. R. Soc. London, Ser. A* **1999**, *455*, 3709.

(93) Yarranton, H.W.; Urrutia, P.; Sztukowski, D.M. Effect of interfacial rheology on model emulsion coalescence (Part II). *J. Colloid Interface Sci.* **2007**, *310*, 253−259.

(94) Dickinson, E. Exploring the frontiers of colloidal behaviour where polymers and particles meet. *Food Hydrocolloids* **2016**, *52*, 497−509.

(95) Yang, F.; Tchoukov, P.; Pensini, E.; Dabros, T.; Czarnecki, J.; Masliyah, J.; Xu, Z. Asphaltene subfractions responsible for stabilizing water-in-crude oil emulsions. Part 1: interfacial behaviors. *Energy Fuels* **2014**, *28*, 6897−6904.

(96) Qiao, P.; Harbottle, D.; Tchoukov, P.; Wang, X.; Xu, Z. Asphaltene subfractions responsible for stabilizing water-in-crude oil emulsions. Part 3. effect of solvent aromaticity. *Energy Fuels* **2017**, *31*, 9179−9187.

(97) Rocha, J. A.; Baydak, E. N.; Yarranton, H. W. What Fraction of the Asphaltenes Stabilizes Water-In-Bitumen Emulsions? Energy Fuels, 2018, 32, 1440−1450. *Energy Fuels* **2018**, *32*, 1440−1450.

(98) Spiecker, P. M.; Gawrys, K. L.; Kilpatrick, P. K. Aggregation and solubility behavior of asphaltenes and their subfractions. *J. Colloid Interface Sci.* **2003**, *267*, 178−193.

(99) Gawrys, K. L.; Spiecker, P. M.; Kilpatrick, P. K. The Role of Asphaltene Solubility and Chemical Composition on Asphaltene Aggregation. *Pet. Sci. Technol.* **2003**, *21*, 461−489.

(100) Stanford, L. A.; Kim, S.; Rodgers, R. P.; Marshall, A. G. Compositional Characterization of Bitumen/Water Emulsion Films by Negative- and Positive-Ion Electrospray Ionization and Field Desorption/Ionization Fourier Transform Ion Cyclotron Resonance Mass Spectrometry. *Energy Fuels* **2006**, *20*, 1664−1673.

(101) Wang, S.; Liu, Q.; Tan, X.; Xu, C.; Gray, M. R. Adsorption of Asphaltenes on Kaolinite as an Irreversible Process. *Colloids Surf., A* **2016**, *504*, 280−286.

(102) Chacon-Patino, M. L.; Moulian, R.; Barrere-Mangote, C.; Putman, J. C.; Weisbrod, C. R.; Blakney, G. T.; Bouyssiere, B.; Rodgers, R. P.; Giusti, P. Compositional Trends for Total Vanadium Content and Vanadyl Porphyrins in Gel Permeation Chromatography Fractions Reveal Correlations between Asphaltene Aggregation and Ion Production Efficiency in Atmospheric Pressure Photoionization. *Energy Fuels* **2020**, *34* (12), 16158−16172.

(103) Raj, G.; Lesimple, A.; Whelan, J.; Naumov, P. Direct Observation of Asphaltene Nanoparticles on Model Mineral Substrates. *Langmuir* **2017**, *33* (25), 6248−6257.

(104) Toulhoat, H.; Prayer, C.; Rouquet, G. CHARACTER-IZATION BY ATOMIC-FORCE MICROSCOPY OF ADSORBED ASPHALTENES. *Colloids Surf., A* **1994**, *91*, 267−283.

(105) Balestrin, L. B. D.; Cardoso, M. B.; Loh, W. Using Atomic Force Microscopy To Detect Asphaltene Colloidal Particles in Crude Oils. *Energy Fuels* **2017**, *31* (4), 3738−3746.

(106) Alshareef, A. H.; Scherer, A.; Tan, X.; Azyat, K.; Stryker, J. M.; Tykwinski, R.; Gray, M. R. Formation of archipelago structures during thermal cracking implicates a chemical mechanism for the formation of petroleum asphaltenes. *Energy Fuels* **2011**, *25*, 2130−2136.

(107) Rueda-Velasquez, R. I.; Freund, H.; Qian, K. N.; Olmstead, W. N.; Gray, M. R. Characterization of asphaltene building blocks by cracking under favorable hydrogenation conditions. *Energy Fuels* **2013**, *27*, 1817−1829.

(108) Habib, F.; Diner, C.; Stryker, J. M.; Semagina, N.; Gray, M. R. Suppression of addition reactions during thermal cracking using hydrogen and sulfide catalyst. *Energy Fuels* **2013**, *27*, 6637−6645.

(109) Gray, M. R.; McCaffrey, W. C. Role of chain reactions and olefin formation in cracking, hydroconversion and coking of petroleum and bitumen fractions. *Energy Fuels* **2002**, *16*, 756−766.

(110) Gaulier, F.; Barbier, J.; Guichard, B.; Levitz, P.; Espinat, D. Asphaltenes Transport into Catalysts under Hydroprocessing Conditions. *Energy Fuels* **2015**, *29* (10), 6250−6258.

(111) Klein, M. T.; Hou, G.; Bertolacini, R.; Broadbelt, L. J.; Kumar, A. *Molecular Modeling in Heavy Hydrocarbon Conversions*; CRC Press: Boca Raton, FL, 2005; p 262.

(112) Miki, Y.; Yamadaya, S.; Oba, M.; Sugimoto, Y. Role of catalyst in hydrocracking of heavy oil. *J. Catal.* **1983**, *83*, 371−383.

(113) Karimi, A.; Qian, K.; Olmstead, W. N.; Freund, H.; Yung, C.; Gray, M. R. Quantitative evidence for bridged structures in asphaltenes by thin film pyrolysis. *Energy Fuels* **2011**, *25*, 3581−3589.

(114) Liao, Z. W.; Zhao, J.; Creux, P.; Yang, C. P. Discussion on the structural features of asphaltene molecules. *Energy Fuels* **2009**, *23*, 6272−6274.

(115) Savage, P. E.; Klein, M. T.; Kukes, S. G. Asphaltene reaction pathways. 1. Thermolysis. *Ind. Eng. Chem. Process Des. Dev.* **1985**, *24*, 1169−1174.

(116) Smith, D. F.; Rodgers, R. P.; Rahimi, P.; Teclemariam, A.; Marshall, A. G. Effect of Thermal Treatment on Acidic Organic Species from Athabasca Bitumen Heavy Vacuum Gas Oil, Analyzed by Negative-Ion Electrospray Fourier Transform Ion Cyclotron Resonance (FT-ICR) Mass Spectrometry. *Energy Fuels* **2009**, *23* (1−2), 314−319.

(117) Furimsky, E. Chemistry of catalytic hydrodeoxygenation. *Catal. Rev.: Sci. Eng.* **1983**, *25*, 421−458.

(118) Chen, H. J.; Massoth, F. E. Hydrodemetalation of vanadium and nickel porphyrins over culfided CoMo/Al₂O₃ catalyst. *Ind. Eng. Chem. Res.* **1988**, *27* (9), 1629−1639.

(119) Barbier, J.; Marques, J.; Caumette, G.; Merdrignac, I.; Bouyssiere, B.; Lobinski, R.; Lienemann, C. P. Monitoring the behaviour and fate of nickel and vanadium complexes during vacuum residue hydrotreatment and fraction separation. *Fuel Process. Technol.* **2014**, *119*, 185−189.

(120) Korre, S. C.; Klein, M. T.; Quann, R. J. Polynuclear Aromatic-Hydrocarbons Hydrogenation. 1. Experimental Reaction Pathways and Kinetics. *Ind. Eng. Chem. Res.* **1995**, *34* (1), 101−117.

(121) Sapre, A. V.; Broderick, D. H.; Fraenkel, D.; Gates, B. C.; Nag, N. K. Hydrodesulfurization of benzo[b]naphtho[2,3 d]thiophene catalyzed by sulfided CoMo MoO₃/γ-Al₂O₃; The reaction network. *AIChE J.* **1980**, *26*, 690−694.

(122) Le Lannic, K.; Guibard, I.; Merdrignac, I. Behavior and Role of Asphaltenes in a Two-stage Fixed Bed Hydrotreating Process. *Pet. Sci. Technol.* **2007**, *25*, 169−186.

(123) Tanaka, R.; Hunt, J. E.; Winans, R. E.; Thiyagarajan, P.; Sato, S.; Takanohashi, T. Aggregates structure analysis of petroleum asphaltenes with small-angle neutron scattering. *Energy Fuels* **2003**, *17*, 127−134.

(124) Sheu, E. Y.; Acevedo, S. Effect of pressure and temperature on colloidal structure of Furrial crude oil. *Energy Fuels* **2001**, *15*, 702−707.

(125) Meille, V.; Schulz, E.; Lemaire, M.; Vrinat, M. Hydrodesulfurization of alkyldibenzothiophenes over a NiMo/Al2O3 catalyst: Kinetics and mechanism. *J. Catal.* **1997**, *170* (1), 29−36.

(126) Hsu, C. S.; Lobodin, V. V.; Rodgers, R. P.; McKenna, A. M.; Marshall, A. G. Compositional Boundaries for Fossil Hydrocarbons. *Energy Fuels* **2011**, *25*, 2174−2178.

(127) Chacón-Patiño, M. L.; Vesga-Martínez, S. J.; Blanco-Tirado, C.; Orrego-Ruiz, J. A.; Gómez-Escudero, A.; Combariza, M. Y. Exploring Occluded Compounds and Their Interactions with Asphaltene Networks Using High-Resolution Mass Spectrometry. *Energy Fuels* **2016**, *30*, 4550−4561.

(128) Nyadong, L.; Lai, J.; Thompsen, C.; LaFrancois, C. J.; Cai, X.; Song, C.; Wang, J.; Wang, W. High-Field Orbitrap Mass Spectrometry and Tandem Mass Spectrometry for Molecular Characterization of Asphaltenes. *Energy Fuels* **2018**, *32*, 294−305.

(129) Chacón-Patiño, M. L.; Blanco-Tirado, C.; Orrego-Ruiz, J. A.; Gómez-Escudero, A.; Combariza, M. Y. Tracing the Compositional Changes of Asphaltenes after Hydroconversion and Thermal Cracking Processes by High-Resolution Mass Spectrometry. *Energy Fuels* **2015**, *29*, 6330−6341.

(130) Neumann, A.; Chacón-Patiño, M. L.; Rodgers, R. P.; Rüger, C. P.; Zimmermann, R. Investigation of island/ single core and archipelago/ multicore enriched asphaltenes and their solubility fractions by thermal analysis coupled to high resolution Fourier-transform ion cyclotron resonance mass spectrometry. *Energy Fuels* **2021**, *35*, 3808−3824.

(131) Gray, M. R.; Tykwinski, R. R.; Stryker, J. M.; Tan, X. Supramolecular assembly model for aggregation of petroleum asphaltenes. *Energy Fuels* **2011**, *25*, 3125−3134.

(132) Murgich, J. Intermolecular forces in aggregates of asphaltenes and resins. *Pet. Sci. Technol.* **2002**, *20*, 983−997.

(133) Groenzin, H.; Mullins, O. C. Asphaltene molecular size and structure. *J. Phys. Chem. A* **1999**, *103* (50), 11237−11245.

(134) Zhang, Y.; Siskin, M.; Gray, M. R.; Walters, C. C.; Rodgers, R. P. Mechanisms of Asphaltene Aggregation: Puzzles and a New Hypothesis. *Energy Fuels* **2020**, *34*, 9094.

(135) Schulze, M.; Lechner, M. P.; Stryker, J. M.; Tykwinski, R. R. Aggregation of asphaltene model compounds using a porphyrin tethered to a carboxylic acid. *Org. Biomol. Chem.* **2015**, *13* (25), 6984−6991.

(136) Schulze, M.; Scherer, A.; Hampel, F.; Stryker, J. M.; Tykwinski, R. R. Synthesis and Aggregation Behavior of Chiral Naphthoquinoline Petroporphyrin Asphaltene Model Compounds. *Chem. - Eur. J.* **2016**, *22* (10), 3378−3386.

(137) Tan, X. L.; Fenniri, H.; Gray, M. R. Pyrene derivatives of 2,2′-bipyridine as models for asphaltenes: Synthesis, characterization, and supramolecular organizations. *Energy Fuels* **2008**, *22* (2), 715−720.

(138) Tan, X. L.; Fenniri, H.; Gray, M. R. Water enhances the aggregation of model asphaltenes in solution via hydrogen bonding. *Energy Fuels* **2009**, *23* (7), 3687−3693.

(139) Wu, J. S.; Fechtenkotter, A.; Gauss, J.; Watson, M. D.; Kastler, M.; Fechtenkotter, C.; Wagner, M.; Mullen, K. Controlled self-assembly of hexa-peri-hexabenzocoronenes in solution. *J. Am. Chem. Soc.* **2004**, *126* (36), 11311−11321.

(140) Pisula, W.; Tomovic, Z.; Simpson, C.; Kastler, M.; Pakula, T.; Mullen, K. Relationship between core size, side chain length, and the supramolecular organization of polycyclic aromatic hydrocarbons. *Chem. Mater.* **2005**, *17* (17), 4296−4303.

(141) Yin, C. X.; Tan, X. L.; Mullen, K.; Stryker, J. M.; Gray, M. R. Associative pi-pi interactions of condensed aromatic compounds with vanadyl or nickel porphyrin complexes are not observed in the organic phase. *Energy Fuels* **2008**, *22* (4), 2465−2469.

(142) Diner, C.; Scott, D. E.; Tykwinski, R. R.; Gray, M. R.; Stryker, J. M. Scalable, Chromatography-Free Synthesis of Alkyl-Tethered Pyrene-Based Materials. Application to First-Generation "Archipelago Model" Asphaltene Compounds. *J. Org. Chem.* **2015**, *80* (3), 1719−1726.

(143) Rybtchinski, B. Adaptive Supramolecular Nanomaterials Based on Strong Noncovalent Interactions. *ACS Nano* **2011**, *5* (9), 6791−6818.

(144) Headen, T. F.; Boek, E. S.; Jackson, G.; Totton, T. S.; Muller, E. A. Simulation of Asphaltene Aggregation through Molecular Dynamics: Insights and Limitations. *Energy Fuels* **2017**, *31* (2), 1108−1125.

(145) Simionesie, D.; O'Callaghan, G.; Laurent, R.; Preece, J. A.; Evans, R.; Zhang, Z. Y. J. Combined Experimental and Computational Study of Polyaromatic Hydrocarbon Aggregation: Isolating the Effect of Attached Functional Groups. *Ind. Eng. Chem. Res.* **2019**, *58* (45), 20505−20515.

(146) Mariani, G.; Moldenhauer, D.; Schweins, R.; Grohn, F. Elucidating Electrostatic Self-Assembly: Molecular Parameters as Key to Thermodynamics and Nanoparticle Shape. *J. Am. Chem. Soc.* **2016**, *138* (4), 1280−1293.

(147) Mariani, G.; Kutz, A.; Di, Z. Y.; Schweins, R.; Grohn, F. Inducing Hetero-aggregation of Different Azo Dyes through Electrostatic Self-Assembly. *Chem. - Eur. J.* **2017**, *23* (26), 6249−6254.

(148) Grohn, F. Soft matter nanoparticles with various shapes and functionalities can form through electrostatic self-assembly. *Soft Matter* **2010**, *6* (18), 4296−4302.

(149) Izzet, G.; Abecassis, B.; Brouri, D.; Piot, M.; Matt, B.; Serapian, S. A.; Bo, C.; Proust, A. Hierarchical Self-Assembly of Polyoxometalate-Based Hybrids Driven by Metal Coordination and Electrostatic Interactions: From Discrete Supramolecular Species to Dense Monodisperse Nanoparticles. *J. Am. Chem. Soc.* **2016**, *138* (15), 5093−5099.

(150) Putman, J. C.; Moulian, R.; Barrere-Mangote, C.; Rodgers, R. P.; Bouyssiere, B.; Giusti, P.; Marshall, A. G. Probing Aggregation Tendencies in Asphaltenes by Gel Permeation Chromatography. Part 1: Online Inductively Coupled Plasma Mass Spectrometry and Offline Fourier Transform Ion Cyclotron Resonance Mass Spectrometry. *Energy Fuels* **2020**, *34* (7), 8308−8315.

(151) Mullins, O. C. The modified Yen model. *Energy Fuels* **2010**, *24*, 2179−2207.

(152) Eyssautier, J.; Levitz, P.; Espinat, D.; Jestin, J.; Gummel, J.; Grillo, I.; Barre, L. Insight into Asphaltene Nanoaggregate Structure Inferred by Small Angle Neutron and X-ray Scattering. *J. Phys. Chem. B* **2011**, *115* (21), 6827−6837.

(153) Dickie, J. P.; Yen, T. F. Macrostructures of the asphaltic fractions by various instrumental methods. *Anal. Chem.* **1967**, *39*, 1847−1852.

(154) Evdokimov, I. N. Colloidal Asphaltenes: Non-extinct "Dinosaurs" in Native Petroleum. *Energy Fuels* **2019**, *33*, 8440−8447.

(155) Barre, L.; Jestin, J.; Morisset, A.; Palermo, T.; Simon, S. Relation between Nanoscale Structure of Asphaltene Aggregates and their Macroscopic Solution Properties. *Oil Gas Sci. Technol.* **2009**, *64* (5), 617−628.

(156) Binks, B. P. Particles as surfactants - similarities and differences. *Curr. Opin. Colloid Interface Sci.* **2002**, *7* (1−2), 21−41.

(157) Nordgard, E. L.; Sorland, G.; Sjoblom, J. Behavior of Asphaltene Model Compounds at W/O Interfaces. *Langmuir* **2010**, *26* (4), 2352−2360.

(158) Yang, F.; Tchoukov, P.; Dettman, H.; Teklebrhan, R. B.; Liu, L.; Dabros, T.; Czarnecki, J.; Masliyah, J.; Xu, Z. H. Asphaltene Subfractions Responsible for Stabilizing Water-in-Crude Oil Emulsions. Part 2: Molecular Representations and Molecular Dynamics Simulations. *Energy Fuels* **2015**, *29* (8), 4783−4794.

(159) Ollinger, J.; Pourmohammadbagher, A.; Quast, A. D.; Becerra, M.; Shumaker-Parry, J. S.; Shaw, J. M. Gold Core Nanoparticle Mimics for Asphaltene Behaviors in Solution and at Interfaces. *Energy Fuels* **2016**, *30* (12), 10148−10160.

(160) Bosman, A. W.; Vestberg, R.; Heumann, A.; Frechet, J. M. J.; Hawker, C. J. A modular approach toward functionalized three-dimensional macromolecules: From synthetic concepts to practical applications. *J. Am. Chem. Soc.* **2003**, *125* (3), 715−728.

(161) Harth, E.; Van Horn, B.; Lee, V. Y.; Germack, D. S.; Gonzales, C. P.; Miller, R. D.; Hawker, C. J. A facile approach to architecturally defined nanoparticles via intramolecular chain collapse. *J. Am. Chem. Soc.* **2002**, *124* (29), 8653−8660.